ABSTRACT

Title of dissertation: NONLINEAR INTERCHANGE MODES
NEAR MARGINAL STABILITY

Jupiter Bagaipo, Doctor of Philosophy, 2013

Dissertation directed by: Professor Adil B. Hassam
Department of Physics

The nonlinear stability of the ideal magnetohydrodynamic interchange mode, at marginal conditions, is studied. The interchange mode is made to be at marginal conditions by providing a constant magnetic field that is just sufficiently strong enough to balance the mode growth. How nonlinearity affects the stability of the interchange mode is analyzed for three different systems. We first consider introducing small amplitude perturbations on a two-dimensional system. We show that if the fractional deviation from marginality is given by a small parameter b, then perturbation amplitudes of order $b^{1/2}$ can cause the system to become nonlinearly unstable. The analysis is corroborated by a nonlinear, compressible, magnetohydrodynamic simulation that shows excellent agreement with the result, including the amplitude scaling. We then extend the analysis to a three-dimensional system where, we show that, the perturbations separate into two different modes. The first mode is shown to be isomorphic to the two-dimensional case and, thus, has the same dynamics, i.e. nonlinearly unstable; however, we show that the second mode is nonlinearly stable. The latter modes are shown to satisfy line-tied boundary condi-

tions. The third system we consider is a two-dimensional system with perturbations introduced as deformations of the boundaries. We show that these small distortions can penetrate deep in the magnetized plasma and become globally amplified. The amplification is shown to be inversely proportional to b. Additionally, we show that nonlinearities can cause the system to become unstable for distortions of order $b^{3/2}$.

NONLINEAR INTERCHANGE MODES NEAR MARGINAL STABILITY

by

Jupiter Anthony G. Bagaipo

Dissertation submitted to the Faculty of the Graduate School of the
University of Maryland, College Park in partial fulfillment
of the requirements for the degree of
Doctor of Philosophy
2013

Advisory Committee:
Professor Adil B. Hassam, Chair/Advisor
Professor James F. Drake
Professor Zackaria Chacko
Dr. Michael M. Swisdak
Professor Christopher S. Reynolds

Dedication

Dedicated to my family.

Acknowledgments

I thank my advisor, Prof. Adil Hassam, for his constant support in this journey and for being a source of inspiration through his enthusiasm in physics and optimism in applying plasma physics for fusion power. It was his enthusiastic nature that made it easy for me to approach him about doing undergraduate research, which, subsequently, introduced me to plasma physics. I also thank Prof. Jim Drake, Prof. Bill Dorland, and Dr. Marc Swisdak for creating such an amazing environment for research and for their willingness to help and answer questions. I also thank these people, along with Prof. Zackaria Chacko and Prof. Chris Reynolds, for taking the time to serve in my thesis committee. I am also grateful for the time I was able to spend doing research with Dr. Parvez Guzdar.

I thank my housemates from IHoP (international house of physicists), past and present: Kevin Schoeffler, Yigit Subasi, Prateek Agrawal, Dinko Ferencek, Zrinka Greguric-Ferencek, Kaushik Mitra, Yigit Subasi, Shannon Brown, Juraj Radic, Kanu Sinha, Ana Jesovnik, Marko Rajkovic, and Dalia Ornelas. Being surrounded by such wonderful people while I am at home has made my graduate experience extraordinary.

Thanks to academic siblings Remington Reid, Bill Young, Ching Pui Hung, Wrick Sengupta, and Lora McMurtrie for the numerous discussions on research or otherwise. Thanks also to my other colleagues, and friends, Brandon Anderson, Pat Harding, Anita Roychowdhury, Shane Squires, Meghan Driscoll, Mark Kegel, Jennifer Elle, Ray Fermo, and Yi-Hsin Liu. Thanks also to Yi-Min Huang and Paul

Cassak for their help and advice on research and careers.

I want to thank Mr. Sean Chappe, my high school physics teacher at Hunterdon Central Regional High School. It is hard to imagine working towards a Ph.D. in physics without his support and guidance. I would also like to thank my best friends Vassili Demergis and Anastasia Pashkova. All of these people were instrumental in my success as a physicist and as a human being, starting back in high school.

I especially thank all my family for their continued support in my choice to do physics and for believing in me. Thanks to my Papa and Mama; to my Ate, her husband Manong Cocoy, and my nephews Binkoy and Niki; to my Manong, his wife Manang Razel, and my nephews Ezee, Amos and Trent; to my Kuya, his wife Ate Neneng, and my nephew DV; and to my Manoy, who I still miss.

I would also like to extend my gratitude to the people outside of the academic setting that helped me throughout my time here. Thanks to my ballroom friends and my rock climbing friends. Thanks to my girlfriend Sonya and all the friends that I met through her.

Table of Contents

List of Figures

List of Abbreviations

β	Plasma Beta (ratio of plasma pressure to magnetic pressure)
ρ	Plasma Density
$\mathbf{u}$	Plasma Velocity
p	Pressure
$\mathbf{J}$	Current
$\mathbf{E}$	Electric Field
$\mathbf{B}$	Magnetic Field
φ	Velocity Stream Function
ψ	Magnetic Stream Function / Flux
Φ	Total Magnetic Flux
$\mathbf{g}$	Gravitational Field
ω	Frequency
$\mathbf{k}$	Wave Number
γ_g	Rayleigh-Taylor Growth Rate
$\mathbf{V_A}$	Alfvén Velocity
ϵ	Smallness Parameter

MHD	Magnetohydrodynamics
2D	Two-Dimensional
3D	Three-Dimensional

Chapter 1

Overview: The Big Picture

1.1 Introduction

Creating a star in a reactor using controlled thermonuclear fusion can be accomplished by a simple sounding process. First, a mix of deuterium and tritium gas is injected into the reactor's vacuum vessel. Next, the gas is ionized to create plasma. Finally, the plasma is heated to a high temperature while maintaining a high density confined for a long enough time for the ions to fuse together. The necessary balance of number density, n, and confinement time, τ_E, to have thermonuclear fusion in a reactor at a temperature, T, is given by the Lawson parameter, $n\tau_E$. At $T \approx 15$ keV, it's required that $n\tau_E \gtrsim 3 \times 10^{14}$ cm^{-3}s.[1, 2, 3]

The inherent challenge in this process is in coming up with a way to stably confine the plasma in order to meet the Lawson criterion. The high temperature means that the plasma must be confined in such a way that it does not touch the walls of the vacuum vessel. Specifically, the heat transport rate from the core to the edge must be low in order to not damage the vessel. Since the plasma is made of particles with electric charge, one possibility would be to use magnetic fields to contain them. The question of plasma confinement then becomes a question of maintaining a high enough β – the ratio of plasma pressure to magnetic pressure.

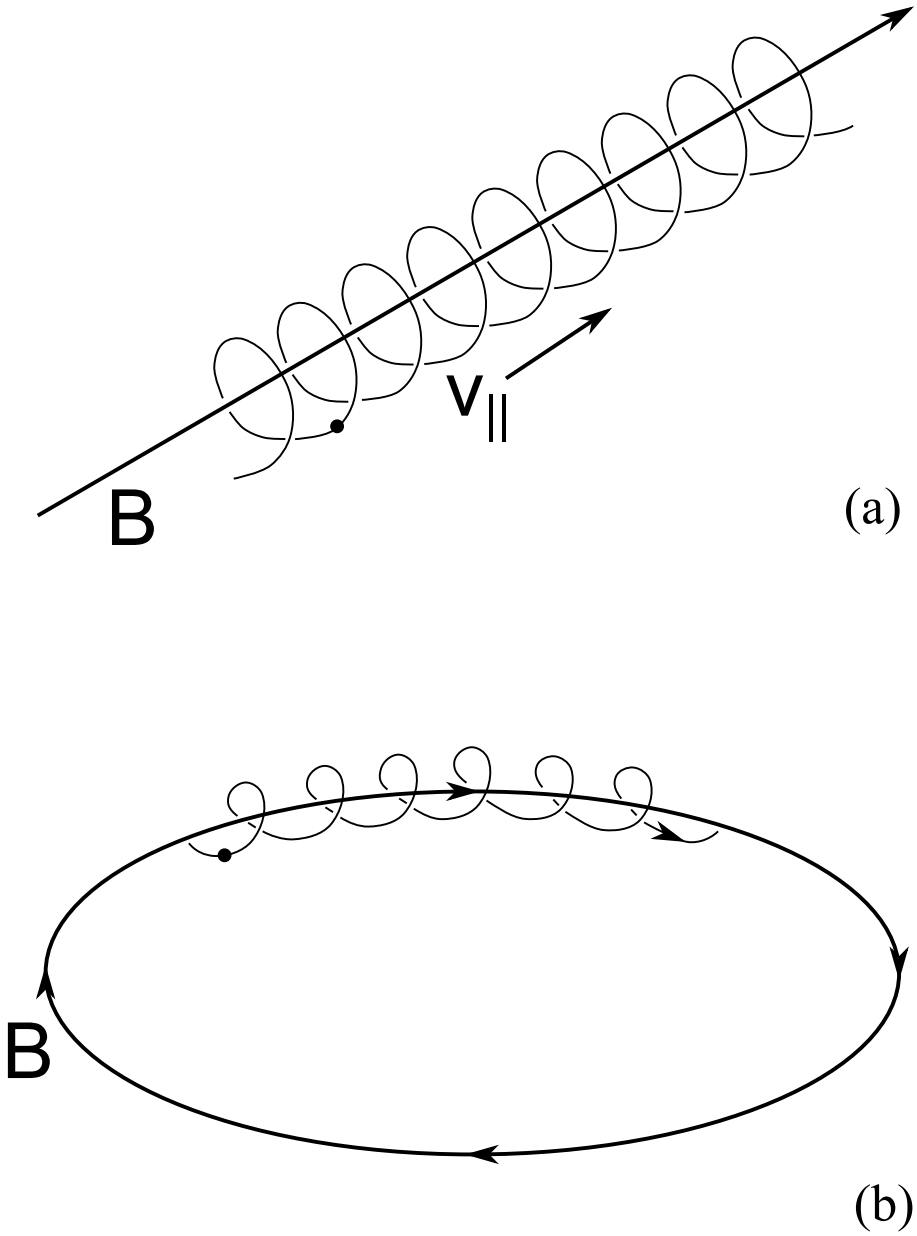

Figure 1.1: The motion of an ion in the presence of a strong magnetic field is shown for (a) a straight magnetic field and (b) a closed magnetic field. For a strong enough magnetic field, the ion Larmor radius is small enough that the motion of the ion is confined to one dimension – parallel to the magnetic field.

1.2 Magnetic Confinement

In order to understand how magnetic fields can be used to confine plasma, we argue as follows. Suppose we have an ion in a vacuum, initially it is able to move freely in three dimensions. If a uniform magnetic field is introduced, then the ion will move in a circular orbit in the plane perpendicular to the direction of the magnetic field. The radius of the circular motion, known as the ion Larmor radius, is inversely proportional to the strength of the magnetic field.[4] So, for a strong enough magnetic field the ion could be effectively confined to one dimension, along the direction of the magnetic field (see Fig. 1.1a). As can be seen in Fig. 1.1b, confinement can be improved further by closing the magnetic field into a loop. Even though this method would be insufficient due to electromagnetic effects, this heuristic discussion, nonetheless, introduces the concept of magnetic confinement of plasma in a simple way.

The next step would be to increase the number of ions in the system so that the density is high enough to meet the Lawson criterion. However, the dynamics of the system changes dramatically as the density is increased and the plasma interacts with the magnetic field. The academic discipline of magnetohydrodynamics (MHD) concerns the study of these dynamics. Using MHD, we can determine different magnetic field configurations that results in an equilibrium. These MHD equilibrium configurations could then be used as a basis in designing a containment device.

Finding an equilibrium is an important step towards fusion, however, it is not sufficient because its stability to small perturbations needs to be determined.

It would not be a very useful containment device if its equilibrium breaks down from small distortions. A lot of work has been done in finding MHD equilibria and analyzing their stability to small perturbations, e.g. Refs. [5, 6, 7]. The result of past findings have led to different containment devices, like tokamaks, reversed field pinches, and stellarators.[2] However, due to the complicated dynamics, stability can only be determined to a certain degree, usually by making some approximations in the system. The idea would be to start the stability analysis with a simple system and then to slowly increase the complexity until the analysis resembles the physical system.

To answer the question of stability, and other questions in MHD, it is necessary to introduce some equations that could be used to model these systems.

1.3 Ideal Magnetohydrodynamics Equations

One set of important equations are the ideal MHD equations. In its entirety, it consists of the continuity equation,

$$\partial_t \rho + \nabla \cdot \rho \mathbf{u} = 0, \tag{1.1}$$

the momentum equation,

$$\rho \frac{d}{dt}\mathbf{u} = -\nabla p + \mathbf{J} \times \mathbf{B}, \tag{1.2}$$

the equation of state,

$$\frac{d}{dt}p + \gamma p \nabla \cdot \mathbf{u} = 0, \tag{1.3}$$

the ideal Ohm's law,

$$\mathbf{E} + \mathbf{u} \times \mathbf{B} = 0, \tag{1.4}$$

and the following Maxwell's equations,

$$\nabla \times \mathbf{E} = -\partial_t \mathbf{B}, \tag{1.5}$$

$$\nabla \times \mathbf{B} = \mu_0 \mathbf{J}, \tag{1.6}$$

$$\nabla \cdot \mathbf{B} = 0, \tag{1.7}$$

where we have

$$\frac{d}{dt} \equiv \partial_t + \mathbf{u} \cdot \nabla, \tag{1.8}$$

and $\gamma = 5/3$ is the ratio of specific heats. The derivation of Eqs. (1.1)-(1.7) is of considerable length, so it will not be presented here; the derivation can be found in Refs. [2, 8]. We will, however, briefly discuss the applicability of the equations and, in the next chapter, we will derive a fundamental result of ideal MHD.

Due to the assumptions required to derive the ideal MHD equations from basic principles, the equations are restricted in their applicability. In general, the ideal MHD equations are valid as long as:

1. The plasma is highly collisional, such that the time scale of collisions is shorter than the characteristic time scales of the system.

2. The ion Larmor radius is much shorter than the characteristic length scales of the system.

3. The resistivity due to collisions is small.

It turns out that despite these limitations, the ideal MHD equations are applicable to a large number of different plasma systems so it is a very useful tool for analysis.

If we are only interested in a specific system (or set of systems) then we can make some further assumptions to simplify the equations.

1.4 Reduced Magnetohydrodynamics Equations

One such simplification is the reduced MHD equations derived by Strauss.[9, 10] The reduced equations consists of the continuity equation,

$$\partial_t \rho + \mathbf{u} \cdot \nabla_\perp \rho = 0, \tag{1.9}$$

the momentum equation (with "gravity" term),

$$\hat{\mathbf{z}} \cdot \nabla_\perp \times (\rho \frac{d}{dt} \mathbf{u}) = \mathbf{B} \cdot \nabla \nabla_\perp^2 \psi + g \partial_y \rho, \tag{1.10}$$

and the flux equation

$$\partial_t \psi - \mathbf{B} \cdot \nabla \varphi = 0, \tag{1.11}$$

where B_z is a constant and φ and ψ define the perpedicular flow and magnetic field, respectively, through the following definitions

$$\mathbf{u} = \hat{\mathbf{z}} \times \nabla_\perp \varphi, \tag{1.12}$$

$$\mathbf{B}_\perp = \hat{\mathbf{z}} \times \nabla_\perp \psi. \tag{1.13}$$

The above equations are derived from the ideal MHD equations in the limit of a large aspect ratio tokamak. In this limit, it is assumed that $B_z \gg B_\perp$, $k_\perp \gg k_z$, and $V_{Az} \gg u$, where u is the typical speed of the plasma and V_{Az} is the Alfvén speed. The "gravity" term models the effect of field line curvature, as will be explained in the next chapter.

In Ref. [9], Strauss took the limit with low β to derive the equations, but the follow-up paper, Ref. [10], extends the derivation to include the case of high β. Remarkably, the two sets of equations are almost identical except for the inclusion of pressure variations in the high β case. In both derivations, the final equations were simplified by taking the case of constant density, however, if density variations are included then we would get Eqs. (1.9)-(1.11). With the use of some hydrodynamic equations, to relate the density and pressure, the reduced equations given by Eqs. (1.9)-(1.11) are applicable to both low and high β cases.

The majority of the analysis in this dissertation will be done using the reduced MHD equations.

1.5 Summary

We gave an overview of the challenge of confining plasma for fusion. We argued, heuristically, that it was possible to accomplish this using magnetic fields but there was a question of stability. The ideal and reduced MHD equations were then presented; these equations could be used to describe the dynamics of plasma in a magnetic field. Analyzing the stability of a certain magnetic configuration using these equations would then be the key to determining its feasibility as a confinement scheme. The validity of the sets of equations were also briefly discussed.

Having established the big picture, we will now focus on analyzing a specific ideal MHD instability – the interchange mode. In Chapter 2, we will give an introduction to the interchange mode and explain how it relates to plasma confinement.

The introduction will be facilitated by a brief analysis with the established linear theory.

In Chapters 3-5 we present our study of the dynamics of the interchange mode near marginal stability. Fusion devices are limited in how intense a magnetic field can be technologically employed. Thus, a system must be designed to operate as close to marginal stability, near a B-threshold, as possible. This is set by stability to the interchange mode. Our initial motivation was that the interchange mode would be weakly convecting when the B-field was slightly below the marginal stability threshold. If this were the case, then it might be acceptable for stellators to be designed for the plasma beta to be slightly above critical as long as the convection was within some tolerance. This could reduce some of the precision tolerances in the design from ideal MHD stability results. Our findings are summarized as follows:

1. First, in Chapter 3, we consider a two-dimensional initial value problem where the plasma is at marginal interchange stability due to a transverse, constant component of the magnetic field. We find that, even in this simple marginal problem, the result was not as expected; instead of weak convection, we find a nonlinearly *unstable* and explosive solution when the transverse B-field was slightly *above* the marginal stability threshold.

2. Next, in Chapter 4, we extend our analysis to a three-dimensional system. The extension is motivated by the fact that the nonlinear instability we found is similar to the "detonation" result of Cowley, et al[11] for a three-dimensional system with line-tying. Our analysis reveals that the three-dimensional sys-

tem can be nonlinearly unstable, but not in the case of line-tied boundary conditions.

3. Finally, in Chapter 5, we return to the two-dimensional case but we look into the effects of boundary perturbations on the nonlinear instability. We study this problem because of a previous result by Adler, et al[12] which found amplification of the marginally stable interchange mode in a system with asymmetric sourcing. We show that the boundary perturbations indeed become amplified in the plasma but that this could induce the nonlinear instability found earlier. This result has the implication that tolerances in magnetic design are likely to be highly sensitive to boundary distortions.

The results of Chapters 3 and 5 are summarized in the publications Refs. [13] and [14], respectively. The results of Chapter 4 are in preparation for submission to the Physics of Plasmas.

Chapter 2

The Interchange Mode

2.1 Introduction

The interchange mode belongs to a class of ideal magnetohydrodynamic instabilities, known as pressure-driven modes – modes driven by the pressure gradient term in the momentum equation. The interchange mode is characterized by the interchange of magnetic flux tubes so that the overall free energy of the system is lowered.[15] The instability occurs when the equilibrium has a density gradient unfavorable to the direction of a "gravitational" force. In systems with curvature, this force comes from a centrifugal force generated by thermal motion along regions of unfavorable curvature. Because of this, the instability is important in fusion devices such as reversed field pinches, stellarators, and tokamaks.[2, 5, 16, 17]

In order to understand how the instability develops it is important to be familiar with a fundamental result of ideal MHD.

2.2 The Frozen-In Theorem

Ohm's law in the ideal MHD equations assumes perfect conductivity for the plasma. As a result of this, a conservation law can be derived for the magnetic flux. This conservation law states that the magnetic flux passing through any open

surface moving with the plasma remains a constant.[2, 18] Explicitly this means that

$$\frac{d}{dt}\Phi = 0, \tag{2.1}$$

where the flux, Φ, is defined as

$$\Phi = \int_S \mathbf{B} \cdot \mathbf{n}\, dS \tag{2.2}$$

for an open surface S moving at the plasma velocity $\mathbf{u}$.

To show Eq. (2.1) we consider the time derivative of Eq. (2.2) for an open surface moving at velocity $\mathbf{v}$. This is given by

$$\frac{d}{dt}\Phi = \int_S \frac{\partial \mathbf{B}}{\partial t} \cdot \hat{\mathbf{n}}\, dS + \oint_{\partial S} \mathbf{B} \cdot \mathbf{v} \times d\mathbf{l}, \tag{2.3}$$

where the first term is the change in flux due to the change in the local magnetic field in S and the second term is the change in flux due to motion of S. The latter can be thought of as the flux through the area swept by an infinitesimal line element $d\mathbf{l}$ moving at velocity $\mathbf{v}$. Using the vector identity $\mathbf{A} \cdot \mathbf{B} \times \mathbf{C} = \mathbf{A} \times \mathbf{B} \cdot \mathbf{C}$ allows us to write Eq. (2.3) in the form

$$\frac{d}{dt}\Phi = \int_S \frac{\partial \mathbf{B}}{\partial t} \cdot \hat{\mathbf{n}}\, dS - \oint_{\partial S} \mathbf{v} \times \mathbf{B} \cdot d\mathbf{l}, \tag{2.4}$$

where we get the minus sign from flipping the cross product. Using Stokes' theorem we can write everything in terms of a surface integral to get

$$\frac{d}{dt}\Phi = \int_S \left(\frac{\partial \mathbf{B}}{\partial t} - \nabla \times (\mathbf{v} \times \mathbf{B}) \right) \cdot \hat{\mathbf{n}}\, dS. \tag{2.5}$$

Combining Faraday's law, Eq. (1.5), and the ideal Ohm's law, Eq. (1.4), implies that Eq. (2.1) follows from Eq. (2.5) if the surface is moving with the plasma, i.e. $\mathbf{v} = \mathbf{u}$.

The means that flux is locally conserved in ideal MHD plasma and, by extension, since the result is for an arbitrary surface, it also implies a global conservation of flux.

A more interesting implication of the result occurs when we consider a "flux tube" – a thin, cylindrical surface with no flux through it, i.e. the magnetic field lines are wrapped as shown in Fig. 2.1. Since all the flux is contained within the surface it drags the magnetic field line with it as it moves with the plasma. Fluid motion can be directly translated to motion of the flux tube which lets us deduce the resulting configuration of the magnetic field lines. This implication gives us an intuitive picture of ideal MHD; the plasma is "frozen in" with the flux tubes. As the plasma flows in the system, the associated magnetic field lines in the flux tube adjust accordingly to conserve the local flux. Since the plasma is a physical object, the frozen-in theorem allows us to treat the magnetic field lines physically, in discussion, by considering the flux tube wrapping them.

For instance, the frozen-in theorem leads to a statement regarding the conservation of magnetic topology in ideal MHD. Inside a flux tube is a connected set of fluid elements that must remain connected for any physically allowable motion of the plasma. That is to say, neighboring fluid elements must remain adjacent to each other. This means that two flux tubes are not allowed to penetrate each other as the ideal MHD system is evolved in time since that involves breaking up adjacent fluid elements. As shown in Fig. 2.2, the resulting state of an initial condition with sheared or crossed flux tubes moving towards each other is the flux tubes getting physically entangled. In ideal MHD theory magnetic topology must be preserved

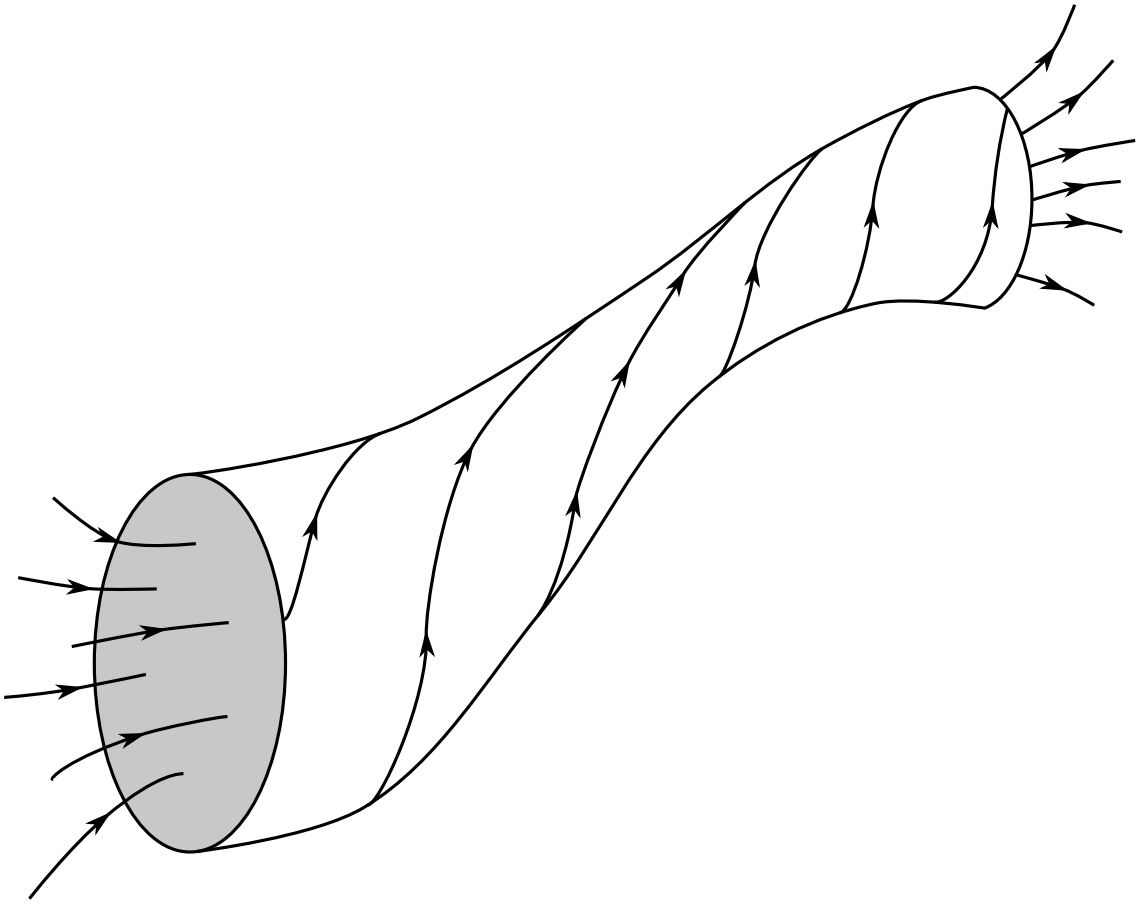

Figure 2.1: Cartoon of a flux tube. The magnetic field lines are contained within or wrapped around the open surface so that there is no component of the magnetic field threading through the surface. The flux tube and magnetic field lines move with the plasma inside the surface.

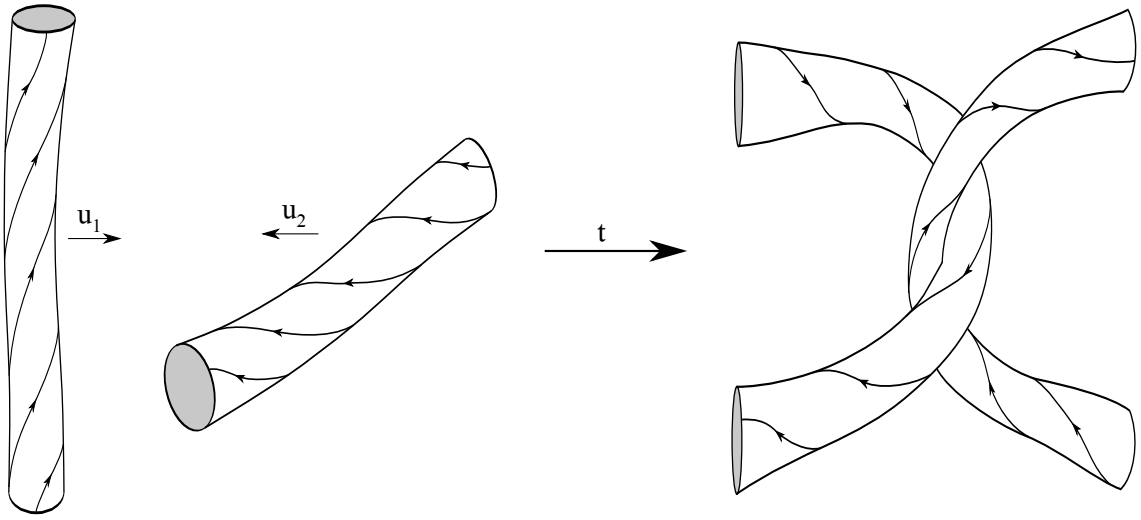

Figure 2.2: Cartoon of the time evolution of two crossed flux tubes, moving towards each other, under ideal MHD. The initial condition shown on the left will evolve, after some time t, to the configuration on the right. The flux tubes do not pass through each other, they are instead tangled together due to the frozen-in theorem.

and the assumptions of ideal MHD need to be broken first before configurations that break topology are allowed.

It is worth noting that this topological constraint can make ideal MHD seem more restrictive because certain configurations that might lower the overall energy of the system are not accessible within the confines of the theory. For instance, reconnection of magnetic field lines is energetically favorable in some MHD systems with magnetic fields in opposing directions, but the only way for reconnection to occur is by introducing a non-ideal term in the theory, e.g. resistivity. Even a small resistivity (to break the ideal Ohm's law) is enough to allow reconnection and dramatically change the overall behaviour of the system.[19, 20] However, these non-ideal effects are usually at a much slower rate that we can still learn some details

about magnetically confined systems in the ideal MHD setting.

Having developed a physical interpretation of the ideal MHD plasma we are now ready to discuss the ideal interchange mode.

2.3 A Physical Description

Consider a heavy (high density) fluid resting "atop" a lighter (less dense) fluid, as shown in Fig. 2.3a. By "atop" we mean that there is a gravitational force acting in the opposite direction of the density gradient. This sets up the well-known Rayleigh-Taylor instability. If the density gradient is steep enough and we create a small perturbation, like in Fig. 2.3b, then the heavier fluid element is going to fall, and continue falling, while the lighter fluid element will rise.[21, 22] Eventually the "bubble" will expand and a convection cell will form that mixes the heavier and lighter fluid elements, as in Fig. 2.3c-d. The signature of this instability is the development of this "mushroom". We introduce this instability as the unmagnetized analog to the interchange instability.

If the fluid were a plasma and we introduced a magnetic field in a direction perpendicular to the density gradient, then the magnetic pressure could support the density gradient. However, this system would still be unstable to the same perturbations because of the frozen-in theorem. As shown in Fig. 2.4, when the heavier plasma falls the flux tube also falls with it, along with the associated magnetic field lines. Since the flux tubes cannot penetrate each other, the flux tube with less density slips aside and interchanges with the falling flux tube; hence the name

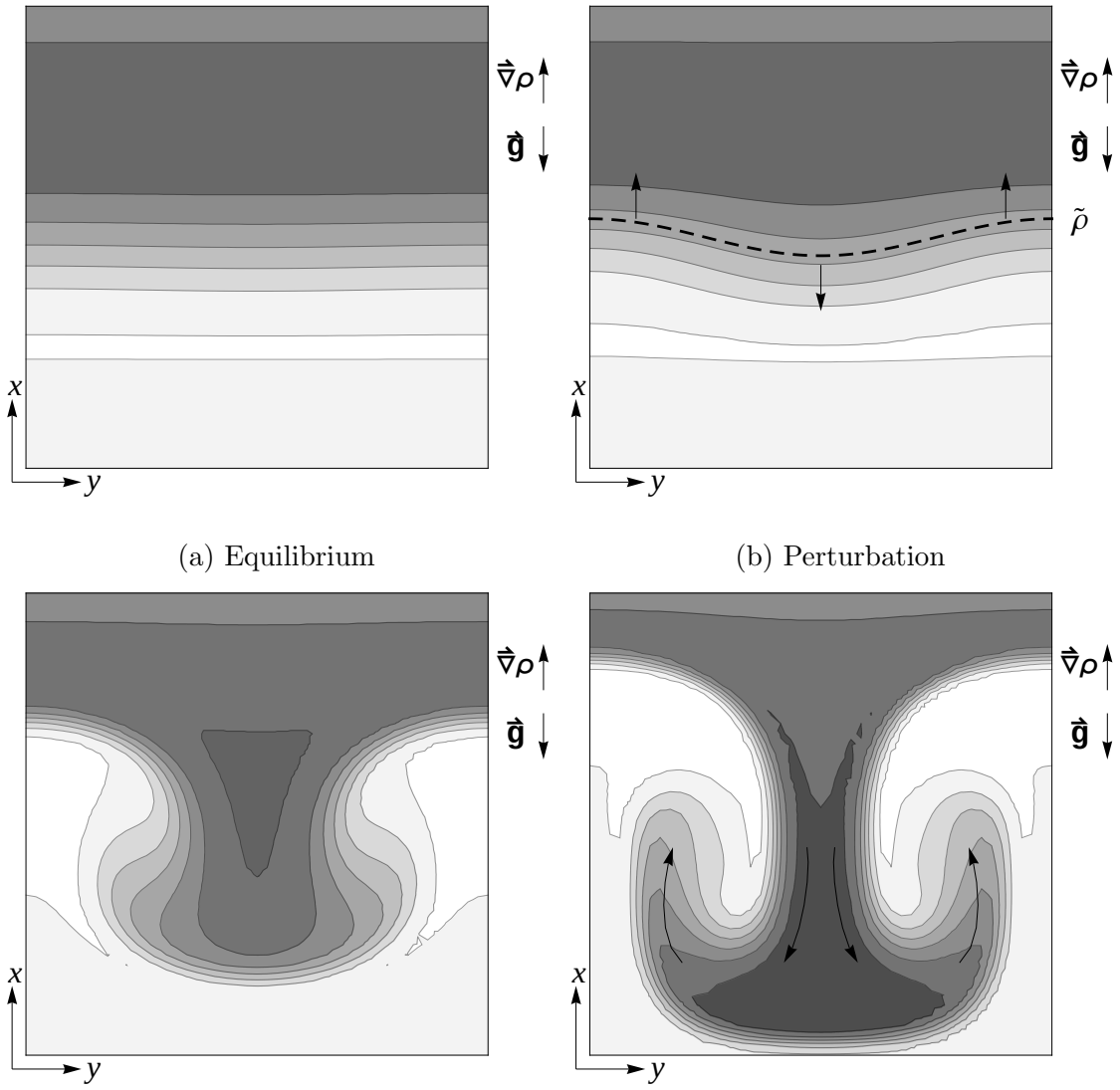

(a) Equilibrium

(b) Perturbation

(c) "Mushroom"

(d) Convection cell

Figure 2.3: Evolution of the Rayleigh-Taylor instability. An unstable equilibrium, (a), is given a small perturbation, (b). The perturbation causes the denser fluid to continue falling, and expands outwards, creating a "mushroom" shape, (c). In linear theory the mode continues to generate convection cells, (d). The plots were created from simulation data.

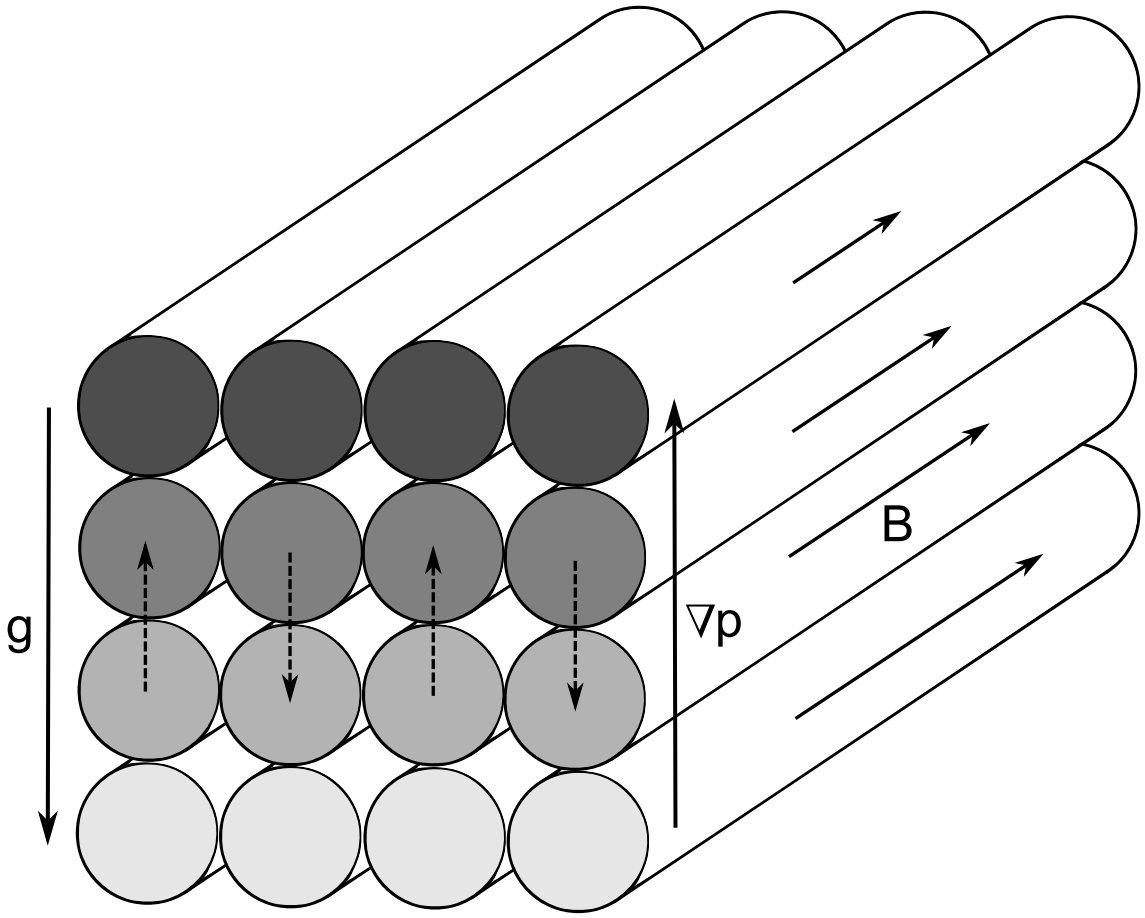

Figure 2.4: Cartoon of a magnetized, Rayleigh-Taylor unstable system. A perturbation on the unstable equilibrium, as denoted by the dashed arrows, results in the interchange mode.

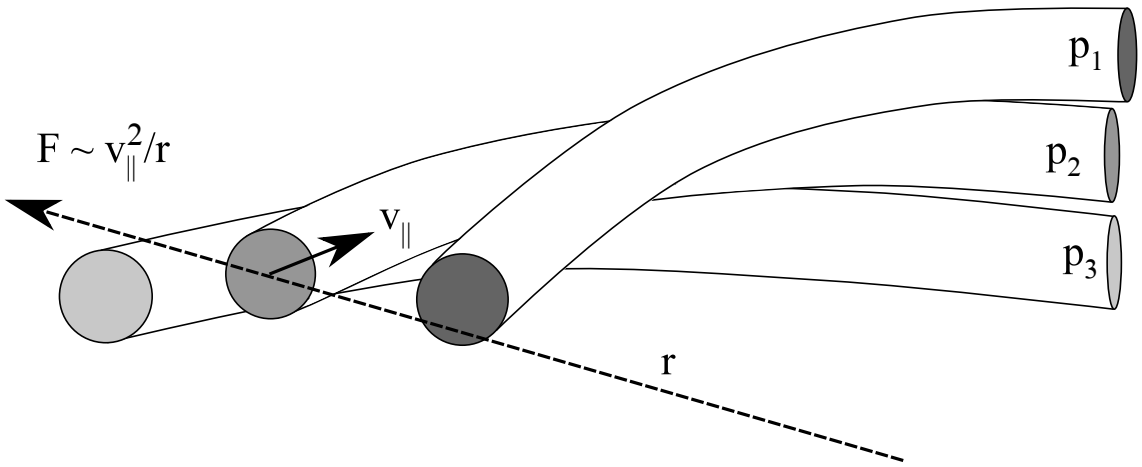

Figure 2.5: Cartoon of a possible flux tube configuration in a toroidal device. Ion thermal motion parallel to the magnetic field, $\mathbf{v}_{\|}$, create an outward centrifugal force. In regions of unfavorable curvature, the pressure gradient is opposite that of the centrifugal force, i.e. $p_1 > p_2 > p_3$, and can be unstable to interchanges.

"interchange" mode. The interchange happens because "lighter" flux tube will fill in the space evacuated by the falling plasma. The interchanges can continue, driven by the inertia of the plasma, to create a convection cell like the Rayleigh-Taylor instability in the unmagnetized fluid case.

In magnetically confined plasma systems, the interchange mode can occur due to the curvature in the magnetic field. With a cross-field pressure gradient, as is likely in these systems, the interchange can go unstable due to forces created by the field line curvature. The average parallel thermal speed (parallel to the magnetic field) causes an outward centrifugal acceleration that can act like the gravitational force in the simplified case. In Fig. 2.5, we can see that if the inner flux tube has a higher pressure than the other flux tubes, i.e. $p_1 > p_2 > p_3$, then an interchange

can occur to lower the overall energy of the system. This instability can destroy the containment of the plasma so it is problematic for magnetic confinement systems.

The interchange mode can be stabilized by introducing a component of the magnetic field transverse to the mode symmetry. This breaks the symmetry of the system and makes it so that the perturbation direction is no longer parallel to the magnetic field. As discussed earlier, because of the frozen-in theorem, sheared flux tubes are not able to penetrate each other and since the flux tubes are no longer aligned they are not able to slip past each other and complete the interchange. The stabilization happens as long as the shear is large enough, i.e. the transverse field is strong enough. Explicitly, the transverse field is required to be large enough that the frequency of the field line bending is greater than the Rayleigh-Taylor growth rate. In other words, magnetic tension is the important parameter in determining the stability of the interchange mode. So, even without a transverse field, the interchange mode can still be stabilized if magnetic tension could be introduced in some other way. One way to do this is to "tie down" the magnetic field lines to some boundary so that an interchange of flux tubes cannot be completed, in much the same way that you cannot interchange two guitar strings. Physically this is accomplished by having hard, conducting plates to create line-tied boundary conditions in the sytem.

With some physical intuition on the behaviour of the interchange mode we will now proceed to discuss exactly what this means in the framework of the ideal MHD theory.

2.4 Mathematical Description: Linear Theory

To fully describe the interchange mode in the context of magnetic confinement requires including the toroidal geometry and shear effects. However, for simplicity, we will be using slab geometry with a constant transverse field. The nonlinear results presented in later chapters were analyzed using this simplified model so we will calculate the linear problem in the same model to appropriately compare them later. While linear theory can be solved in the more complicated system (still not completely though), the nonlinear problem is significantly more difficult to make progress. As is usually the case in physics, the hope is that we can gain some insight in this simpler problem that can be used to help solve the more complete problem.

We will first briefly derive the linear result using the full set of ideal MHD equations. This allows us to then show that the result can be recovered in the context of reduced MHD. For brevity, both derivations will be sparse on details; they are only included for completeness in introducing the interchange mode and not meant to be a full description of linear theory. A more complete description can be found elsewhere, e.g. Ref. [2, 8].

2.4.1 Using full ideal MHD equations

Consider an equilibrium with

$$p = p_0(x), \quad \rho = \rho_0(x), \quad \mathbf{B} = B_{z0}(x)\hat{\mathbf{z}} + B_{y0}\hat{\mathbf{y}}, \quad \mathbf{u} = 0. \tag{2.6}$$

As mentioned earlier, the driving force in the interchange instability is the centrifugal force from field curvature. In slab geometry we model this effect by a gravitational field, $\mathbf{g} = -g\hat{\mathbf{x}}$ ($g \sim v_{thi}^2/R$, where R is the radius of curvature), that acts on the density. Adding this gravitational force in Eq. (1.2), we get

$$\partial_x(p_0 + \frac{1}{2\mu_0}B_{z0}^2) = -g\rho_0 \tag{2.7}$$

as the equilibrium condition.

Linearizing the ideal MHD equations about the equilibrium given in Eq. (2.6) yields the following relevant equations for the perturbed quantities:

$$\partial_t\tilde{\rho} + \rho_0'\tilde{u}_x + \rho_0\nabla\cdot\tilde{\mathbf{u}} = 0, \tag{2.8}$$

$$\hat{\mathbf{z}}\cdot\nabla\times(\rho_0\partial_t\tilde{\mathbf{u}}) = \frac{1}{\mu_0}B_{y0}\hat{\mathbf{z}}\cdot\nabla\times\partial_y\tilde{\mathbf{B}} + g\partial_y\tilde{\rho}, \tag{2.9}$$

$$\hat{\mathbf{z}}\cdot\nabla\times\partial_t\tilde{\mathbf{B}} = B_{y0}\hat{\mathbf{z}}\cdot\nabla\times\partial_y\tilde{\mathbf{u}} - B_{y0}(\nabla\cdot\tilde{\mathbf{u}})', \tag{2.10}$$

$$\partial_t\tilde{B}_z = B_{y0}\partial_y\tilde{u}_z - B_{z0}\nabla\cdot\tilde{\mathbf{u}} - B_{z0}'\tilde{u}_x, \tag{2.11}$$

$$\partial_t\tilde{p} + p_0'\tilde{u}_x + \gamma p_0\nabla\cdot\tilde{\mathbf{u}} = 0, \tag{2.12}$$

where the primes denote a derivative in x. In order to show clearly the stabilization by a transverse field,[1] variations in z are suppressed, i.e. $\partial_z = 0$. Since parallel wavenumbers are stabilizing, we can just deduce the effect of reintroducing variations in z to the final result. An advantage of doing this is that it allows us to use the operators $\hat{\mathbf{z}}\cdot\nabla\times$ and $\hat{\mathbf{z}}\cdot$ to simplify some of the equations.

[1]Henceforth, we will take the $\hat{\mathbf{z}}$ and $\hat{\mathbf{y}}$ directions to be the "parallel" and "transverse" direction, respectively.

In order to make some progress, we assume that the system is incompressible so that

$$\nabla \cdot \tilde{\mathbf{u}} = 0. \tag{2.13}$$

This assumption of incompressibility is actually a result that can be shown explicitly by combining Eqs. (2.11) and (2.12) and going through some rigorous asymptotics with the ansatz that

$$\omega(\tilde{p} + \frac{1}{\mu_0} B_{z0} \tilde{B}_z) \ll g\rho_0 \tilde{u}_x. \tag{2.14}$$

Equation (2.13) follows from taking the low β and large radius of curvature limits in addition to the limit with $B_{y0} \ll B_{z0}$. The ansatz is found to be self-consistent in the short wavelength limit with sub-magnetosonic frequencies. More details on this calculation can be found in Ref. [8].

Substituting Eq. (2.13) into Eqs. (2.8)-(2.10), and taking the limit of short wavelength and localized perturbations, yields the eigenvalue problem

$$\rho_0 \partial_t^2 \partial_y \tilde{u}_x = \frac{1}{\mu_0} B_{y0}^2 \partial_y^3 \tilde{u}_x + g\rho_0 \partial_y \tilde{u}_x \tag{2.15}$$

for $\tilde{u}_x$. After writing $\tilde{u}_x = u_x(x) \exp(ik_y y - i\omega t)$, we arrive at the short wavelength, low β, local dispersion relation

$$\omega^2 = V_{Ay}^2 k_y^2 - \gamma_g^2, \tag{2.16}$$

where

$$V_{Ay} = \frac{B_{y0}^2}{\mu_0 \rho_0} \tag{2.17}$$

is the Alfvén speed and

$$\gamma_g^2 = g\rho_0'/\rho_0 \tag{2.18}$$

is the local Rayleigh-Taylor growth rate. As we expected in the discussion in Sec. 2.3 the interchange mode is stabilized ($\omega^2 > 0$) when the transverse field (B_{y0}) is strong enough that the restoring frequency from field line bending ($k_y V_{Ay}$) can overcome the Rayleigh-Taylor growth rate. Stabilization by parallel wavenumbers will result in

$$\omega^2 = V_{Az}^2 k_z^2 - \gamma_g^2, \tag{2.19}$$

instead. This completes the derivation of the linear interchange mode dispersion relation using the full ideal MHD equations.

2.4.2 Using reduced MHD equations

In arriving at Eq. (2.16) it was necessary to make several assumptions in order to arrive at a complete set of equations that can lead to a solution. The process can be simplified greatly if we instead start with the reduced MHD equations given by Eqs. (1.9)-(1.11) where, as we showed in the previous chapter, some of the assumptions are already incorporated in the equations, e.g. large aspect ratio.

The equilibrium, in the context of reduced MHD equations, is given by

$$\rho = \rho_0(x), \quad \mathbf{B} = B_0 \hat{\mathbf{z}} + B_{y0} \hat{\mathbf{y}}, \quad \varphi = 0, \tag{2.20}$$

which means $\psi_0 = B_{y0} x$. We linearize the reduced MHD equations about this equilibrium to get

$$\partial_t \tilde{\rho} - \rho_0' \partial_y \tilde{\varphi} = 0, \tag{2.21}$$

$$\partial_t (\rho_0' \tilde{\varphi}' + \rho_0 \nabla_\perp^2 \tilde{\varphi}) = (B_0 \partial_z + B_{y0} \partial_y) \nabla_\perp^2 \tilde{\psi} + g \partial_y \tilde{\rho}, \tag{2.22}$$

$$\partial_t \tilde{\psi} = (B_0 \partial_z + B_{y0} \partial_y) \tilde{\varphi}, \tag{2.23}$$

Combining the above equations and taking the short wavelength and local limits yields

$$\rho_0 \partial_t^2 \tilde{\varphi} = (B_0 \partial_z + B_{y0} \partial_y)^2 \tilde{\psi} + g \rho_0' \tilde{\varphi}. \tag{2.24}$$

Finally, a Fourier transform on $\tilde{\varphi}$ leads to the dispersion relations given in Eqs. (2.16) and (2.19) for $k_z = 0, B_{y0} \neq 0$ and $k_z \neq 0, B_{y0} = 0$, respectively.

2.5 Summary

An overview of the linear theory of the ideal MHD interchange mode was given. We first showed that the ideal Ohm's law assumption of ideal MHD results in a conservation law for the magnetic flux, called the frozen-in theorem. This fundamental result of ideal MHD allowed us to develop a physical intuition for the behaviour of magnetic field in a magnetized plasma system; the most important of which is the idea of flux tubes and conservation of magnetic topology. This result meant that the introduction of a straight magnetic field perpendicular to the gravitational force does not alter the Rayleigh-Taylor instability because the flux tubes will just interchange. However, because magnetic topology is conserved, transverse magnetic fields can stabilize the interchange of flux tubes. We finished the physical description discussion of the interchange mode by claiming that the key feature of the interchange mode is the interplay of the stabilization due to the magnetic tension and the unstable growth due to the Rayleigh-Taylor instability.

After learning what to expect from the physical behaviour of the interchange

mode, we proved how this comes about from a mathematical standpoint using two sets of equations: the full ideal MHD equations and the reduced MHD equations. A few assumptions had to be invoked in order to arrive at a solution using the full ideal MHD equations, the most useful of which is the incompressibility assumption. The final result was an agreement with the physical analysis – the growth rate of the interchange mode was driven by the Rayleigh-Taylor growth rate and stabilized by the Alfvénic wave frequency. We learned that the calculation could be made considerably easier by using the reduced equations, since they are already simplified by the same assumptions.

In this dissertation, we study systems where the interchange mode is stabilized with a transverse field or line-tied boundary conditions. However, it should be noted that stabilization can be achieved by other means. In particular, one such mechanism comes from the Rayleigh-Taylor growth rate that drives the destabilization of the interchange mode. We showed that $\gamma_g^2 = g\rho_0'/\rho_0$; however, this result assumes that $p_0'/\gamma p_0 \ll \rho_0'/\rho_0$, that is to say, it assumes that the scale size of of the density is much shorter than the scale size of the pressure. If this was not the case then the growth rate is given by $\gamma_g^2 = g(\rho_0'/\rho_0 - p_0'/\gamma p_0)$.[8] Thus, even if $\rho_0'/\rho_0 > 0$, the system could still be stable to interchange modes if the pressure profile was such that $p_0'/\gamma p_0 > \rho_0'/\rho_0$. In general, this mechanism has importance in solar and astrophysical systems, but not so much in conventional laboratory fusion plasma systems that we are studying. Other stabilizing effects worth mentioning, that are not included in this study, are the previously mentioned magnetic shear and velocity shear.

Now that we have an understanding of the linear theory of interchange modes, we will now focus our attention on nonlinear analysis. We start with a two-dimensional initial value problem.

Chapter 3

Two-Dimensional Nonlinear Instability

3.1 Introduction

We learned, in the previous chapter, that it is well-known that the MHD magnetized plasma interchange instability can be stabilized by a transverse magnetic field. For a given wavenumber, allowing a magnetic field component in the direction of the wavenumber introduces Alfvénic stabilizing tension such that beyond a critical transverse field (transverse to the direction of mode symmetry) that wavenumber is linearly stable.[2] The nonlinear evolution of the magnetized plasma interchange instability is less well understood. In particular, the state of the system for when the transverse B-field is marginally subcritical (or, equivalently, the plasma beta is slightly above critical) is an important question for magnetized fusion energy applications: does the mode saturate at low amplitude and how does the marginal convection and resulting transport scale with deviation from marginality? The question is an important consideration for stellarators, for example, since these fusion devices are engineered for very high precision magnetic fields and one of the precision constraints arises from ideal MHD linear stability results.[17] If the nonlinear consequence of a slightly subcritical B-field were better understood, it may be possible to optimize over the MHD design constraints. It was also recently shown that the linear growth rate of ideal interchanges in a reversed-field pinch

for a slightly subcritical B-field is weaker than expected and may be overcome by nonlinear effects.[23]

There have been a few studies done on nonlinear growth of interchange instabilities at marginal stability in tokamaks.[24, 25, 26, 11, 27, 28] Although a Lagrangian approach has been attempted,[29] the general approach is to expand the equation of motions of the unstable mode about marginal stability and thus the nonlinear terms in the system can be evaluated.[25, 26] We can determine the overall stability of the system by comparing the behaviour of the nonlinear effects to the linear driving term. In Ref. [25] the author found that, for the profiles investigated, the nonlinear effects were stabilizing. Similarly, in Ref. [26] the author showed nonlinear saturation at marginal stability. Both authors considered a system with a sheared magnetic field. In studying the line-tied g mode, the authors in Ref. [11] showed that near the marginally stable point the system was nonlinearly unstable. However, Refs. [27, 28] showed that the nonlinear growth transitions through an initial regime where the nonlinear growth dominates the linear response, as shown in Ref. [11], but a secondary regime takes over when the amplitude is sufficiently large and so the mode amplitude remains bounded.

We simplify our system to a slab geometry where we use an effective gravitational field, $\mathbf{g}$, to model centrifugal force due to field line curvature[15] and we assume a constant transverse field. This reduces the complexity of the system so that the focus of the analysis can be on how nonlinear terms get introduced into the equations of motion. The idealized system is described in Sec. 3.2 along with the derivation of nonlinear time evolution equation. The goal is to have a simpler

methodology in a simple system that can be generalized into more complicated systems, e.g. sheared field[30], ballooning[31, 32], etc. In Sec. 3.3 we verify our result using a dissipative numerical simulation. The results are summarized in Sec. 3.4.

3.2 Analytic Theory

As we showed in Chapter 1, if we consider a slab system with constant gravity $\mathbf{g} = -g\hat{\mathbf{x}}$ and very strong magnetic field in the z direction such that $B_\perp \ll B_z$ and V_{Az} is much larger than the typical flow in the system then this system is found to be incompressible and can be described by the two-dimensional MHD reduced equations. We rewrite them here for convenience:

$$\partial_t \rho + \mathbf{u} \cdot \nabla_\perp \rho = 0, \tag{3.1}$$

$$\hat{\mathbf{z}} \cdot \nabla_\perp \times (\rho \frac{d}{dt}\mathbf{u}) = \mathbf{B}_\perp \cdot \nabla_\perp \nabla_\perp^2 \psi + g\partial_y \rho, \tag{3.2}$$

$$\partial_t \psi - \mathbf{B}_\perp \cdot \nabla_\perp \varphi = 0, \tag{3.3}$$

where $\mathbf{u} = \hat{\mathbf{z}} \times \nabla_\perp \varphi$ and $\mathbf{B}_\perp = \hat{\mathbf{z}} \times \nabla_\perp \psi$ and we have defined, in the usual way,

$$\frac{d}{dt} \equiv \frac{\partial}{\partial t} + \mathbf{u} \cdot \nabla_\perp.$$

Variations in z are suppressed since the fastest interchange has $\partial/\partial z = 0$. The nonlinear system of equations given by Eqs. (3.1)-(3.3) can be solved for the variables ρ, the density, and φ and ψ, the flow and magnetic streamfunctions, respectively.

We consider a static equilibrium with a density gradient that's unstable to interchange and a constant, transverse magnetic field. More explicitly, we have

$$\rho_0'(x) > 0, \quad \mathbf{B}_\perp = B_0 \hat{\mathbf{y}}, \quad \varphi_0 = 0, \tag{3.4}$$

where henceforth the primes denote differentiation with respect to x. We also add the assumption that $\rho_0' \to 0$ at the boundaries and has even parity.

As shown in the previous chapter, small perturbations about this equilibrium yield the WKB dispersion relation

$$\omega^2 = k^2 V_{Ay}^2 - \gamma_g^2 \tag{3.5}$$

where $\gamma_g = |g\rho'/\rho|^{1/2}$ is the Rayleigh-Taylor growth rate and k is the wavenumber in the y direction. In this chapter, we consider the dynamics of the magnetized interchange mode when the magnetic field strength is strong enough to just stabilize interchanges, i.e., the system is near marginal stability. In particular, for a given k, suppose $\omega^2 > 0$ everywhere in x except for a single small region where it is very close to zero, positive or negative. In that case, weakly growing perturbations are possible in the vicinity of where $k^2 V_{Ay}^2 - \gamma_g^2$ is close to zero. The time rate of change of the perturbations will be very small compared to the local γ_g. Thus, we order

$$\partial_t / \gamma_g \sim \epsilon \ll 1. \tag{3.6}$$

This implies that any deviations in B_0 away from criticality must be small. In particular, if

$$B_0 = B_c + b_2 \tag{3.7}$$

then, according to Eq. (3.5), b_2/B_c must be of $\mathcal{O}(\epsilon^2)$.

We allow small perturbations about this marginal point such that the amplitude of the magnetic perturbation, A, while small, is large enough that the nonlinear magnetic tension forces can influence the growth time. This results in the optimal

ordering

$$A/\psi_0 \sim \epsilon. \tag{3.8}$$

We represent the perturbation by expanding ψ and φ in a series

$$\psi = \psi_0 + \psi_1 + \psi_2 + \psi_3 + \cdots \tag{3.9}$$

$$\varphi = \varphi_1 + \varphi_2 + \varphi_3 + \cdots \tag{3.10}$$

where the order in ϵ is denoted by the subscript. The continuity equation, Eq. (3.1), can be satisfied by letting $\rho = \rho(\psi)$ and using Eq. (3.3). With this change of variable we can expand ρ in terms of $\delta\psi = \psi - \psi_0$ to get

$$\rho(\psi) = \rho_0 + \frac{\rho_0'}{B_0}\delta\psi + \frac{1}{2}\frac{\rho_0''}{B_0^2}\delta\psi^2 + \frac{1}{6}\frac{\rho_0'''}{B_0^3}\delta\psi^3 + \cdots . \tag{3.11}$$

Substituting the expansions given by Eqs. (3.9)-(3.11) into Eqs. (3.2) and (3.3) we can solve for the nonlinear evolution of the perturbations order by order.

3.2.1 First order equations

Matching terms to lowest, non-vanishing order, we obtain from Eqs. (3.2) and (3.3) the equations

$$0 = B_c\partial_y\nabla_\perp^2\psi_1 + g\partial_y\rho_1, \tag{3.12}$$

$$-B_c\partial_y\varphi_1 = 0, \tag{3.13}$$

where Eq. (3.11) gives

$$\rho_1 = \rho_0'\psi_1/B_c. \tag{3.14}$$

Substituting ρ_1 into Eq. (3.12) the equation becomes

$$\mathcal{L}(\psi_1) = 0 \tag{3.15}$$

where we have defined the operator

$$\mathcal{L}(f) \equiv (\nabla_\perp^2 + \frac{g}{B_c^2}\rho_0')\partial_y f.$$

Writing ψ_1 as

$$\psi_1(x, y, t) = A(t)\zeta_1(x)\cos(ky), \tag{3.16}$$

we obtain the eigenvalue equation

$$\zeta_1''(x) - k^2\zeta_1(x) + \frac{g}{B_c^2}\rho_0'\zeta_1(x) = 0 \tag{3.17}$$

that can be solved to get an eigenvalue for B_c. The boundary condition for ρ_0 implies that ζ_1 decays exponentially close to the boundary.

In writing Eq. (3.16) we assumed a cosine perturbation in the density which implies $\psi_1 \sim \cos(ky)$ from Eq. (3.11). If we also assume that this initial perturbation results in a pure mode for the lowest order flow then

$$\varphi_1(x, y, t) = 0 \tag{3.18}$$

is the solution to Eq. (3.13).

To the lowest order we have found that given the mode of the density perturbation, k, and the equilibrium density gradient profile, $\rho_0'(x)$, then the marginally stable field strength B_c can be solved for using Eq. (3.17). This result is consistent with the prediction from linear theory for the existence of the marginally stable value.

3.2.2 Second order equations

In order to solve for the time evolution of ψ_1, it is necessary to proceed to higher order in the expansion. We now match $\mathcal{O}(\epsilon^2)$ terms in Eqs. (3.2) and (3.3) to get

$$B_c\partial_y\nabla_\perp^2\psi_2 + g\partial_y\rho_2 + \mathbf{B}_1\cdot\nabla_\perp\nabla_\perp^2\psi_1 = 0, \tag{3.19}$$

$$\partial_t\psi_1 = B_c\partial_y\varphi_2, \tag{3.20}$$

where Eq. (3.11) to the same order gives

$$\rho_2 = \frac{\rho_0'}{B_c}\psi_2 + \frac{1}{2}\frac{\rho_0''}{B_c^2}\psi_1^2. \tag{3.21}$$

Using ψ_1 from Eq. (3.16), φ_2 can be solved for in Eq. (3.20) to obtain

$$\varphi_2(x,y,t) = \frac{1}{kB_c}\frac{dA(t)}{dt}\zeta_1(x)\sin(ky) + \bar{\varphi}_2(x,t), \tag{3.22}$$

where $\bar{\varphi}_2(x,t)$ is a constant of integration.

Substituting Eq. (3.21) into Eq. (3.19) results in an equation for ψ_2,

$$\mathcal{L}(\psi_2) = -\frac{g}{B_c^3}\rho_0''\partial_y(\psi_1^2), \tag{3.23}$$

where we have used Eq. (3.15) to simplify the Laplacian. This has a solution of the form

$$\psi_2(x,y,t) = A(t)^2\zeta_2(x)\cos(2ky) + \bar{\psi}_2(x,t), \tag{3.24}$$

where $\bar{\psi}_2(x,t)$ is the homogeneous solution to Eq. (3.23). Substituting Eq. (3.24) into Eq. (3.23), we find $\zeta_2(x)$ satisfies

$$\zeta_2''(x) - 4k^2\zeta_2(x) + \frac{g}{B_c^2}\rho_0'\zeta_2(x) = -\frac{1}{2}\frac{g}{B_c^3}\rho_0''\zeta_1(x)^2. \tag{3.25}$$

To fully analyze the stability of our system we still have to resolve the time evolution of ψ_1. It is also important to solve for $\bar{\psi}_2$ and $\bar{\varphi}_2$ to make sure that those terms are well-behaved.

3.2.3 Third order equations

As was done previously in lower orders, we match terms of $\mathcal{O}(\epsilon^3)$ in Eqs. (3.2) and (3.3). The resulting higher order equations are

$$\partial_t(\rho_0\nabla_\perp^2\varphi_2 + \rho_0'\varphi_2') = B_c\partial_y\nabla_\perp^2\psi_3 + b_2\partial_y\nabla_\perp^2\psi_1$$
$$+ g\partial_y\rho_3 + \mathbf{B}_1\cdot\nabla_\perp\nabla_\perp^2\psi_2 + \mathbf{B}_2\cdot\nabla_\perp\nabla_\perp^2\psi_1 \tag{3.26}$$

$$\partial_t\psi_2 = B_c\partial_y\varphi_3 + \mathbf{B}_1\cdot\nabla_\perp\varphi_2 \tag{3.27}$$

along with

$$\rho_3 = \frac{\rho_0'}{B_c}\psi_3 - \frac{\rho_0' b_2}{B_c^2}\psi_1 + \frac{\rho_0''}{B_c^2}\psi_1\psi_2 + \frac{1}{6}\frac{\rho_0'''}{B_c^3}\psi_1^3 \tag{3.28}$$

from Eq. (3.11).

Integrating Eq. (3.26) over one period in y we find that $\bar{\varphi}_2$ is not driven by ψ_1 so we can set

$$\bar{\varphi}_2(x,t) = 0 \tag{3.29}$$

without loss of generality. No zonal flows are generated in the system when creating a periodic perturbation in the density. However, averaging Eq. (3.27) over y we find that zonal fields are generated according to

$$\bar{\psi}_2(x,t) = \frac{1}{2}\frac{1}{B_c}A(t)^2\zeta_1(x)\zeta_1'(x). \tag{3.30}$$

For a given k and ρ_0 the system is now solved up to second order with the exception of the time evolution of $A(t)$. The variables ψ_1, φ_1, ψ_2, and φ_2 are defined by Eqs. (3.16), (3.18), (3.24), and (3.22), respectively. We can solve for ζ_1 using Eq. (3.17) and then for ζ_2 using Eq. (3.25). The y-independent terms $\bar{\varphi}_2$ and $\bar{\psi}_2$ are given by Eqs. (3.29) and (3.30).

To solve for $A(t)$ we need to simplify Eq. (3.26) by making use of Eqs. (3.15), (3.20), and (3.28). After some algebra Eq. (3.26) takes the form

$$\frac{1}{k^2 B_c}\partial_t^2\left(\frac{g}{B_c^2}\rho_0\rho_0'\partial_y\psi_1 - \rho_0'\partial_y\psi_1'\right) = \\ B_c\mathcal{L}(\psi_3) - 2\frac{g}{B_c^2}b_2\rho_0'\partial_y\psi_1 + \mathcal{F}[\psi_1,\psi_2], \tag{3.31}$$

where exact details of the functional $\mathcal{F}$ is suppressed here for clarity but is shown in Appendix A. We can extract a time evolution equation by substituting Eqs. (3.16), (3.24), and (3.30) into the above equation and applying the operator $\int dx\,\zeta_1(x)\int d(cos(ky))$ evaluated over all space. This operation will annihilate the ψ_3 term and any higher order harmonics.

After simplification (see Appendix A), we arrive at the equation for $A(t)$

$$\frac{1}{k^2 B_c}\langle\rho_0\rho_0'\zeta_1^2\rangle\frac{d^2}{dt^2}A(t) = -2b_2\langle\rho_0'\zeta_1^2\rangle A(t) \\ + \left(\langle\rho_0''\zeta_1^2\zeta_2\rangle - \frac{1}{4}\frac{1}{B_c}\langle\rho_0'\zeta_1^2(\zeta_1^2)''\rangle - \frac{1}{4}\frac{B_c}{g}\langle\zeta_1^2(\zeta_1^2)''''\rangle\right)A(t)^3, \tag{3.32}$$

where the angled brackets are defined as

$$\langle f\rangle \equiv \frac{1}{L_\rho}\int dx\, f(x)$$

with $L_\rho^{-1} \equiv \rho_0'/\rho_0$ evaluated at $x = 0$. We can simplify this further by letting

$$x \to \chi L_\rho,$$

$$\rho_0(x) \to \rho_0(0)\rho(\chi),$$

$$\zeta_1(x) \to Z_1(\chi),$$

$$\zeta_2(x) \to Z_2(\chi)/(B_c L_\rho),$$

in order to introduce dimensionless versions of the variables x and ρ_0, and have A with dimensions of ψ. Applying this normalization to Eq. (3.32) we get

$$\frac{1}{k^2 V_{Ac}^2}\frac{d^2}{dt^2}A(t) = -2\frac{b_2}{B_c}c_1 A(t) + \frac{c_3}{B_c^2 L_\rho^2}A(t)^3 \tag{3.33}$$

where $V_{Ac}^2 \equiv B_c^2/\rho_0(0)$ and

$$c_1 = \frac{\langle \rho' Z_1^2 \rangle}{\langle \rho\rho' Z_1^2 \rangle}, \tag{3.34}$$

$$c_3 = \frac{\langle \rho'' Z_1^2 Z_2 \rangle}{\langle \rho\rho' Z_1^2 \rangle} - \frac{1}{4}\frac{\langle \rho' Z_1^2 (Z_1^2)'' \rangle}{\langle \rho\rho' Z_1^2 \rangle} - \frac{1}{4}\frac{V_{Ac}^2}{gL_\rho}\frac{\langle Z_1^2 (Z_1^2)'''' \rangle}{\langle \rho\rho' Z_1^2 \rangle}, \tag{3.35}$$

where the primes and brackets now denote derivatives and integrals in χ. Using the same normalization on Eqs. (3.17) and (3.25) we get the following equations,

$$Z_1'' - k^2 L_\rho^2 Z_1 + \frac{gL_\rho}{V_{Ac}^2}\rho' Z_1 = 0, \tag{3.36}$$

$$Z_2'' - 4k^2 L_\rho^2 Z_2 + \frac{gL_\rho}{V_{Ac}^2}\rho' Z_2 = -\frac{1}{2}\frac{gL_\rho}{V_{Ac}^2}\rho'' Z_1^2, \tag{3.37}$$

for the dimension-free Z_1 and Z_2.

The equation for the time evolution given by Eq. (3.33) closes the system and we can fully determine the first and second order perturbations, ψ_1 and ψ_2 defined

by Eqs. (3.16) and (3.24), for a given k, ρ_0, and b_2. This is achieved by first solving the eigenvalue problem Eq. (3.36) and using the solution for Z_1 and B_c to solve for Z_2 using Eq. (3.37), and finally determining the coefficients defined by Eqs. (3.34) and (3.35), and solving for $A(t)$ in Eq. (3.33).

The coefficient c_1 is a positive number for $\rho' > 0$, and so the linear stability of the system is determined by the sign of b_2. This result agrees with the linear theory. However, the overall nonlinear stability of the system is going to be determined largely from the sign of c_3 compared to the sign of b_2.

3.2.4 Short wavelength limit

We can analytically solve Eq. (3.36) for the case $kL_\rho \gg 1$ in which regime the cells are elongated in x direction but still shorter than the scale of the gradient, i.e.,

$$kL_\rho \gg \chi^{-1} \gg 1.$$

With this scaling we can approximate $\rho'(\chi)$ to be

$$\rho'(\chi) \approx 1 - \frac{\chi^2}{2}. \tag{3.38}$$

Assuming that $gL_\rho/V_{Ac}^2 \sim k^2 L_\rho^2$, then from scaling arguments we find that Eq. (3.36) has the familiar form of a quantum harmonic oscillator. This has the well-known solution

$$Z_1(\chi) = \hat{Z}_1 \exp\left(-\frac{kL_\rho}{2\sqrt{2}}\chi^2\right), \tag{3.39}$$

$$k^2 L_\rho^2 = \frac{gL_\rho}{V_{Ac}^2}\left(1 - \frac{1}{\sqrt{2}}\frac{1}{kL_\rho}\right), \tag{3.40}$$

for the ground state. This solution is correct only for $kL_\rho \gg 1$ and the solution for the "energy" adds a small correction to the initial assumption. Using the same scaling, to lowest order, Eq. (3.37) has the solution

$$Z_2(\chi) = -\frac{1}{6}\chi Z_1(\chi)^2. \tag{3.41}$$

The time evolution equation given by Eq. (3.33) can be simplified in the $kL_\rho \gg 1$ limit by substituting the solutions Eqs. (3.39)-(3.41) in the coefficients given by Eqs. (3.34) and (3.35). After simplification we arrive at the following values for the coefficients

$$c_1 = 1, \quad c_3 = \frac{1}{8}kL_\rho \tag{3.42}$$

where we only kept the largest terms and have assumed that $\hat{Z}_1 = 1$.

The above result implies that even if $b_2 > 0$, if the initial amplitude $A_0 \equiv A(0)$ is such that

$$\frac{A_0}{B_c L_\rho} > 4\sqrt{\frac{b_2}{B_c}\frac{1}{kL_\rho}}, \tag{3.43}$$

then the system will be nonlinearly unstable and the amplitude will increase without bound. Furthermore, for $b_2 < 0$ the instability grows faster than predicted from linear theory and any small perturbation will continue to grow larger without saturation.

With the solution for the eigenmode we can check the ratio between the spatial scale of the perturbation, characterized by the displacement in the x direction ξ_x, and the width of the eigenmode

$$\Delta \sim \sqrt{\frac{L_\rho}{k}}, \tag{3.44}$$

given by Eq. (3.39). The displacement is related to the velocity by $\partial_t \xi_x \sim u_x$, and from Eq. (3.20) we get that $\partial_t A \sim B_c u_{x2}$, which implies that $A \sim B_c \xi_x$. Substituting for A using Eq. (3.43) gives us a scale for the displacement,

$$\xi_x \sim \sqrt{\frac{b_2}{B_c}\frac{L_\rho}{k}} \tag{3.45}$$

which yields

$$\frac{\xi_x}{\Delta} \sim \sqrt{\frac{b_2}{B_c}} \tag{3.46}$$

for the ratio of the two scale lengths. As should be expected, the spatial size of the amplitude required to be nonlinearly unstable is much smaller than the width of the eigenmode.

3.3 Numerical Simulation

To confirm this result, we used a two-dimensional code that solves the fully compressional equations. A short description of the code and the equations solved are shown in Appendix B. The variables ρ, $\rho\mathbf{u}$, ψ, and B_z are solved numerically and stepped in time. We set $B_z \gg |B_\perp|$ so the equations are effectively reduced. The code is dissipative so we introduced source terms in the density in order to maintain a steady state profile suitable for our model. The sourcing, although weak, results in a profile for $B_y(x)$. To compare with analytic theory, we wish to keep B_y approximately constant. Thus, we allowed B_z to resistively relax at a somewhat slower rate than B_y in the equilibrium.

The system is normalized so that initially $V_{Az} = 1$ and $L_x = 1$, where L_x is the height of the box. We used hardwall, free-slip boundary conditions for the

top and bottom walls and periodic boundary conditions for the sides. The periodic boundary conditions discretize the system so that the only wavenumbers allowed are integer multiples of $2\pi/L_y$, where L_y is the width of the box. From Eq. (3.5) we know that the lower modes are the most unstable, so to study the case with $kL_\rho \gg 1$, i.e. short wavelength, we selected L_y such that the minimum value for kL_ρ satisfies this condition. By choosing $k = 2\pi/L_y$ we can satisfy the marginality condition by adjusting B_0 and/or g such that $kV_{Ay} \approx \gamma_g$ for the minimum mode. We set $L_y = 0.5$, and from the density profile we have $L_\rho = \rho_0/\rho_0' \approx 0.4$ and so we satisfy the condition

$$kL_\rho \approx 5.03 \gg 1$$

which is necessary to compare with the analytical result from Sec. 3.2.4. We attempted to run tests with a larger value of k by decreasing L_y, but the code was numerically unstable for smaller box widths.

To generate the equilibrium we initialize ψ to $B_0 x$ and let the system reach an equilibrium which is steady state. The density source term results in a weak flow in the x direction. This flow scales with the diffusion, so a minimal, numerically-stable value for the diffusion is chosen to minimize its effect. The equilibrium profiles for the density and the background field generated are shown in Fig. 3.1. It is important to note that the equilibrium profile for the density does not have $\rho_0' \to 0$ at the boundaries. The boundary conditions imply that $\rho_0' \to -g\rho_0$ at the wall.

After the equilibrium is made, a density perturbation is introduced with $\tilde{\rho}(x, y) = a_0 \cos(ky)$. From Eq. (3.14) we can relate the density perturbation ampli-

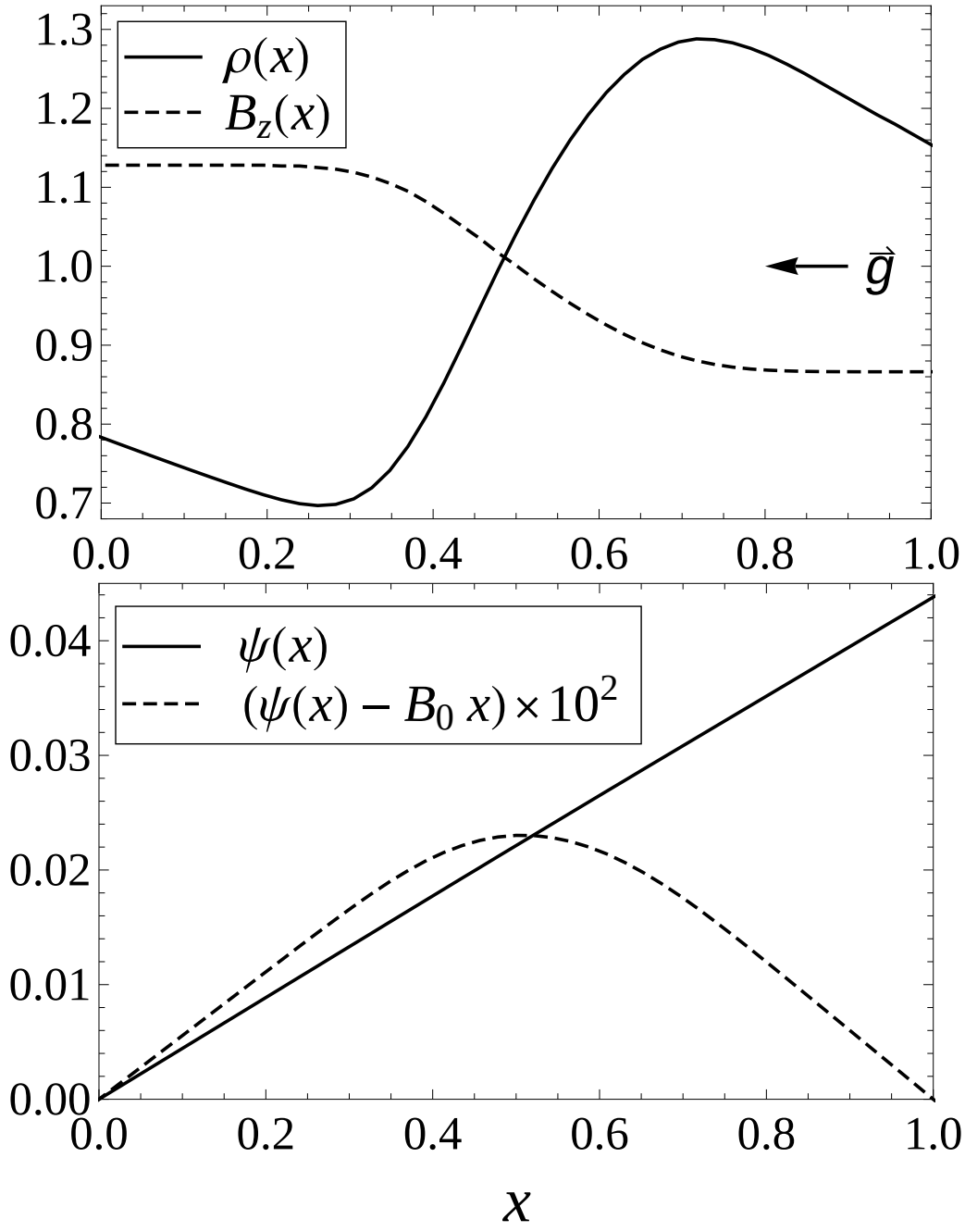

Figure 3.1: The equilibrium profiles for the background field B_z, the density ρ, and the magnetic streamfunction ψ along with the difference from constant field.

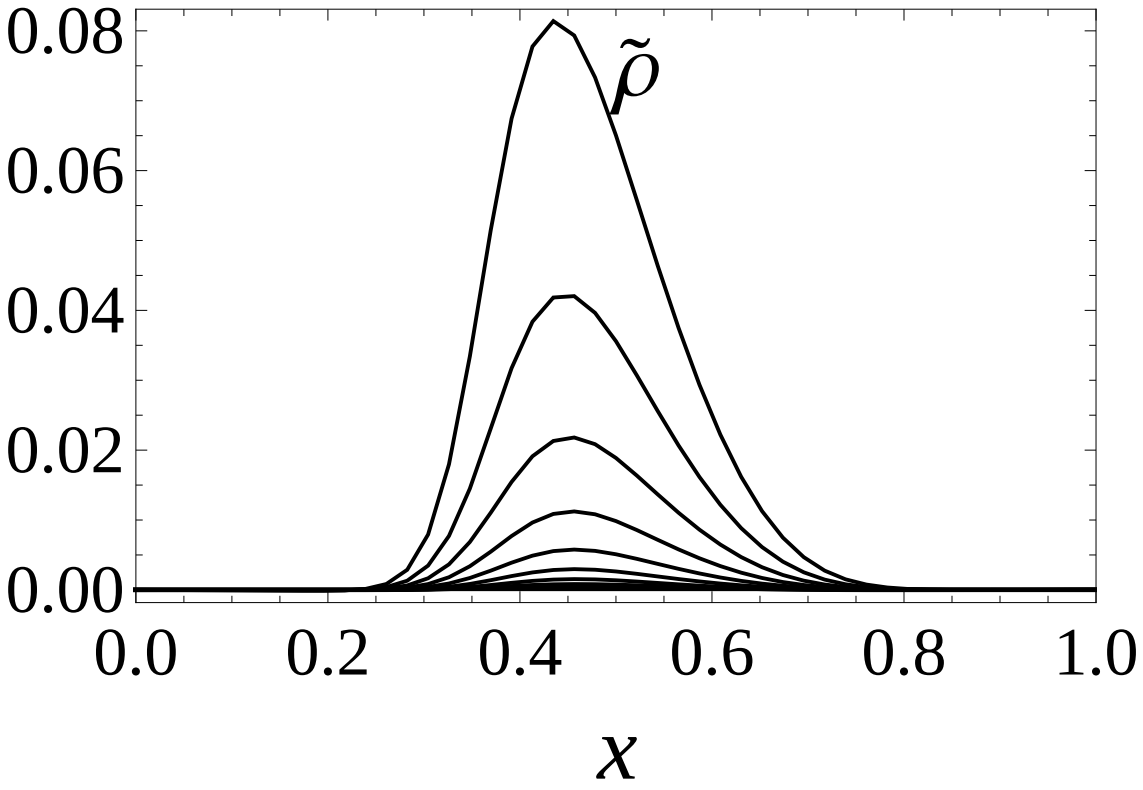

Figure 3.2: The linear growth of an unstable localized mode cut at $y \approx 0.26$ and for $t \leq 60\tau_A$. Time traces separated by $t \approx 6\tau_A$ are shown.

tude, $a(t)$, to the perturbation amplitude of ψ, i.e. $a = \rho_0' A/B_c$. In Fig. 3.2 we show the resulting unstable eigenmode developing for the density. For tests done with B_0 far away from marginality, i.e. $|b_2/B_c| \approx 50\%$, there was excellent agreement for the growth rate/frequency in the simulation with Eq. (3.5). The theory predicts that there will be nonlinear coupling to the mode with wavenumber $2k$, so it is important that this mode and higher modes are allowed. Since the diffusivity is weak, it is ensured that this is the case.

Since we can adjust both B_0 and g to achieve marginal stability, we decided to fix the value of g at 0.15, and adjust B_0. With this value of g we expect that $B_c \approx 0.05$ based on Eq. (3.40). However, we found that an equilibrium with $B_0 = 0.05$ is stable to perturbations as large as $a_0 = 10^{-1}$ in the simulation. We decreased the strength of the transverse field until it became unstable to perturbations with $a_0 = 10^{-4}$. This value was at $B_0 \approx 0.0438$ and we took this to be the critical value of the transverse field for the numerical simulation. Since the critical amplitude scales like the square root of the deviation from marginality, we are limited to perturbations only as small as 10^{-4} otherwise smaller perturbations would have meant having deviations that are close to the limits of our computational power.

We created multiple equilibria with different transverse field strength within 10% of the numerical critical field strength. These equilibria were then perturbed with a_0 of different orders of magnitude. The result of the test is shown in Fig. 3.3 where circles and crosses mark stable and unstable points, respectively, and the solid line is for $a_0 = 4\rho_0'\sqrt{(b_2/B_c)(L_\rho/k)}$, from our theory, using the parameters from the numerical simulation. The slope of the theory line seems consistent with

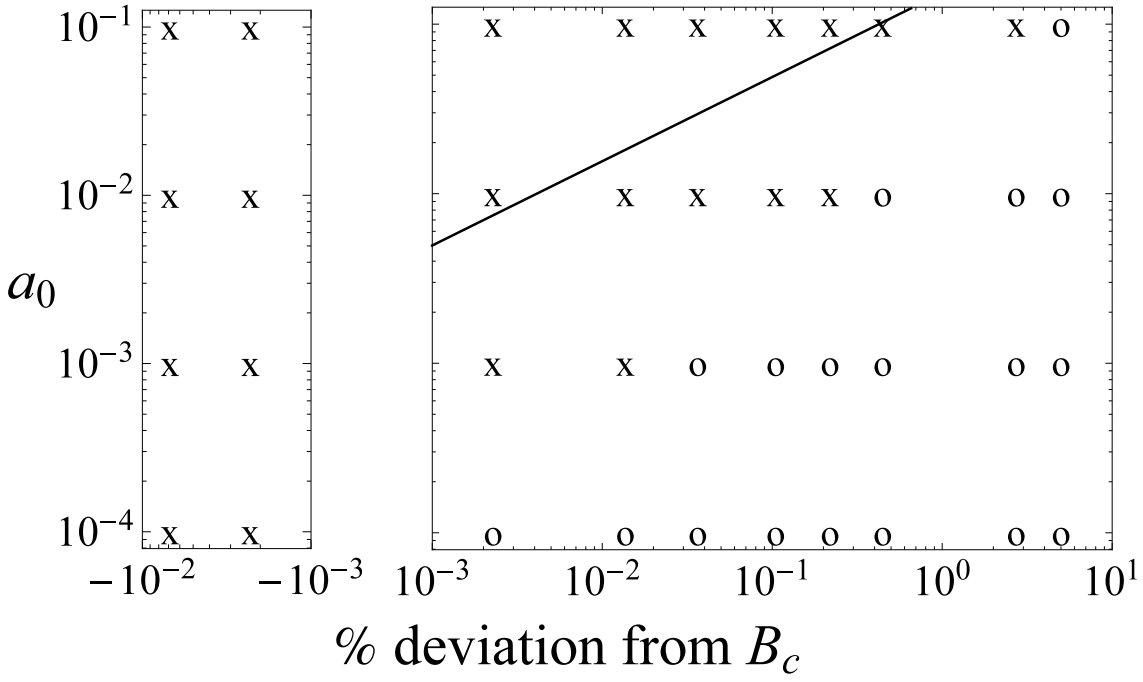

Figure 3.3: Result of stability test for a range of deviations from B_c and magnitude of perturbation, a_0. Stable and unstable results are denoted by a circle or a cross, respectively. The solid line is the theoretical boundary.

the numerical data, however, the theory requires larger a_0 for nonlinear instability. This inconsistency could be due to the diffusion in the code and, in particular, the resistivity may allow for slippage in the magnetic field lines which can shift the stability boundary at marginal stability. We can calculate the scale size of this shift based on the values used in the simulation (see Appendix B),

$$\frac{\eta/\Delta^2}{kV_{Ay}} \approx 2.5\%. \tag{3.47}$$

This implies that there could be a shift in B_c of order $\sqrt{b_2/B_c}$. At marginal stability, even small diffusion can cause significant shifts in stable-unstable boundaries. However, this implies a shift in B_c; it is harder to explain why resistivity results in a nonlinear instability at large amplitude of perturbation. It is possible that diffusive effects may affect the critical amplitude for nonlinear instability, but the existence of a nonlinear instability phenomenon is harder to explain as a diffusive effect.

In addition to checking the perturbations for a growing linear mode, we also check the time trace of the amplitude for nonlinear effects. In Fig. 3.4 we show a time trace of the amplitude of $\tilde{\rho}$, $a(t)$, for the same B_0 but different a_0. We can see that the behaviours are different for the two cases. In the unstable case, Fig. 3.4a, the density perturbations become very large quickly and eventually dissipate after it hits the boundaries ($t \lesssim 100\tau_A$). The time trace of ρ' shows that the density profile flattens out ($\rho' \to 0$) after reaching a peak. So, even though our analysis in Sec. 3.2 is only valid as long as $A \lesssim \epsilon$ we can see from the trace that it continues beyond this limit until the profile collapses. The stable case, Fig. 3.4b, has an initial growth eventually hitting a peak and then has stable oscillations. Even though the

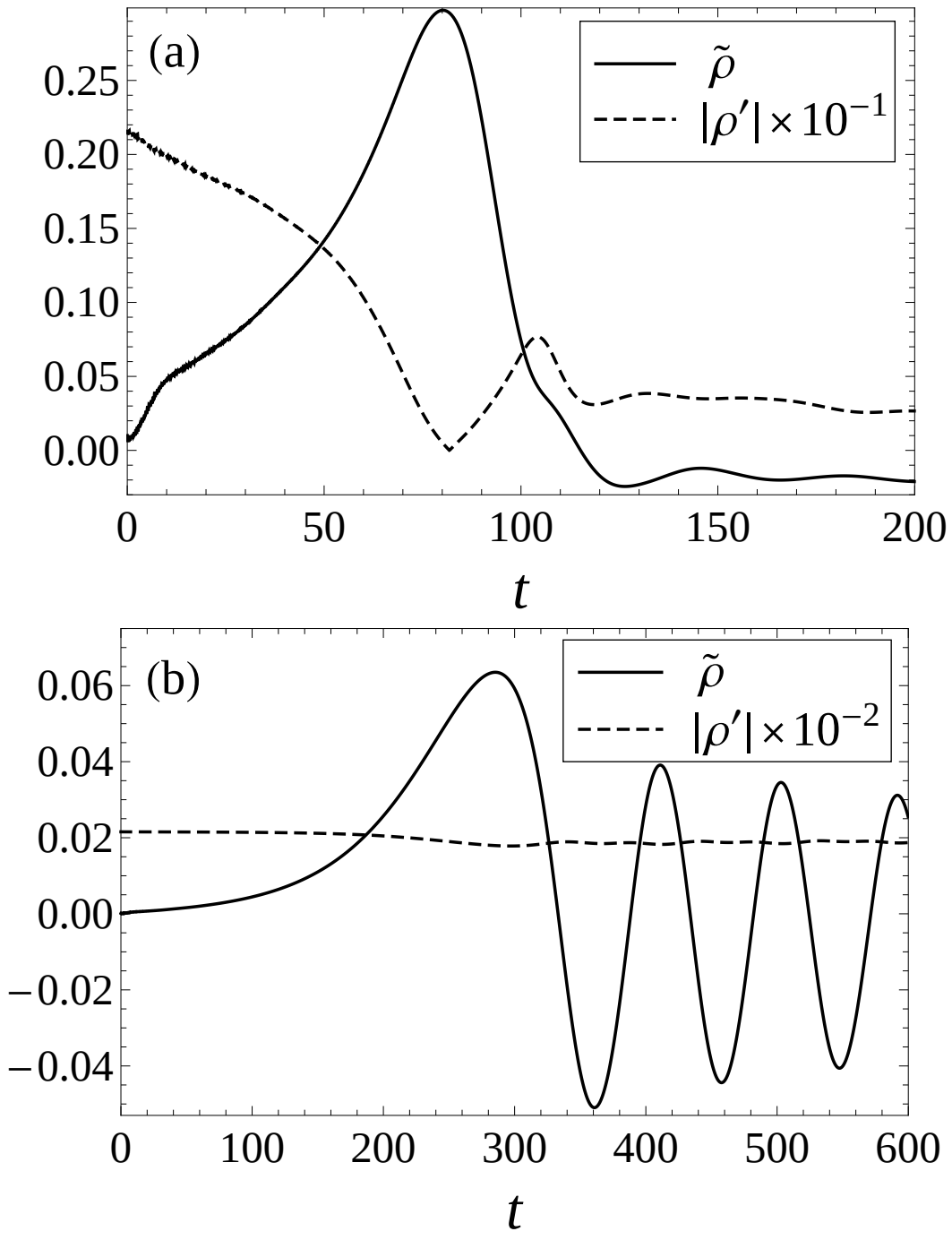

Figure 3.4: Time trace of the amplitude of density perturbations $\tilde{\rho}$ (solid line) and x derivative of the density ρ' (dashed line) for $b_2/B_c \approx 0.04\%$ with (a) $a_0 = 10^{-2}$ and (b) $a_0 = 10^{-4}$.

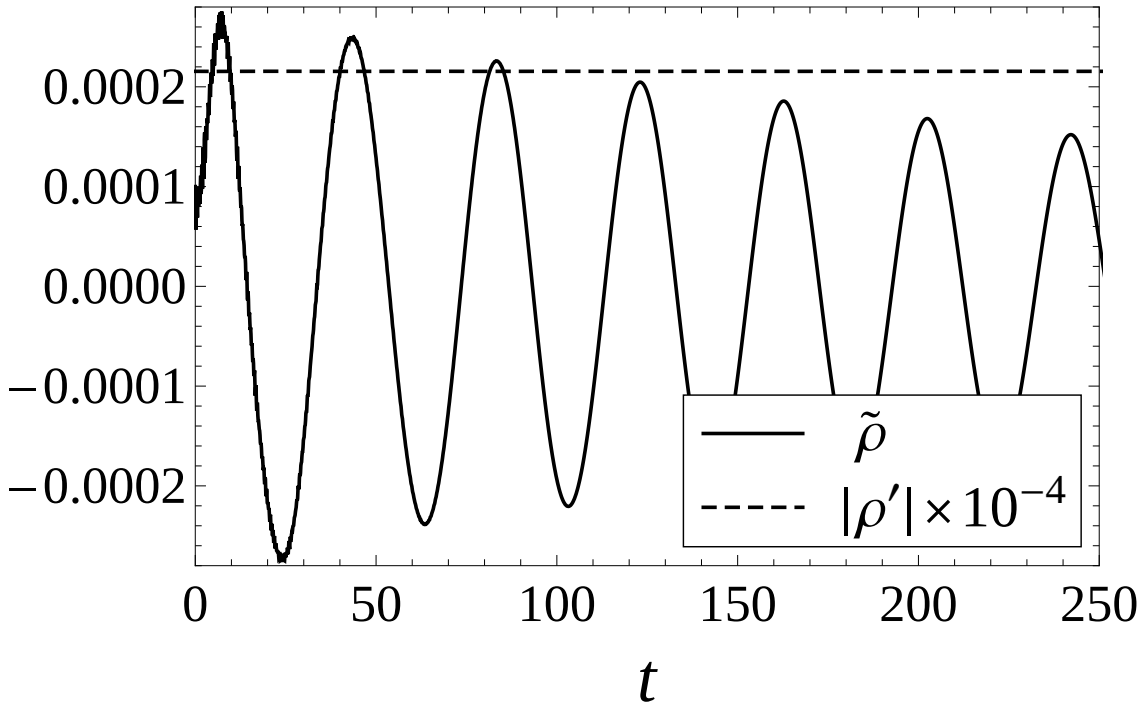

Figure 3.5: Time trace of the amplitude of density perturbations $\tilde{\rho}$ (solid line) and x derivative of the density ρ' (dashed line) for $b_2/B_c \approx 10\%$ with $a_0 = 10^{-4}$.

amplitude increases some, it is still small and the density profile holds. This can be seen from the fact that ρ' is staying constant the entire time. We can see in Fig. 3.5 that as we increase b_2/B_c further from marginality, this initial growth decreases in magnitude. It also develops faster and has more noise that is indicative of a transient oscillatory mode.

3.4 Summary and Conclusions

In this chapter, we studied the nonlinear behaviour of a marginally stable interchange system. We used the reduced equations to find an analytic solution near marginality given a density profile, $\rho_0(x)$, deviation from marginality, b_2, and wavenumber of perturbation, k, of the B-field. The result is a nonlinear differential equation for the amplitude of the density perturbations as a function of time. The threshold for nonlinear instability is dependent on the above quantities, along with g. The principal finding is that marginally stable interchange modes in a magnetized plasma can be nonlinearly unstable for large enough initial perturbations. We arrived at this result from a systematic asymptotic expansion about marginality in the smallness parameter, $|b_2/B_c|^{1/2}$, carried out to third order. The first order solution can be found using the linear eigenvalue problem. This solution is then used as a source for the second order problem. The third order analysis yields the equation for the time dependence of the perturbation. We found that the stability of the solution can be determined by calculating the coefficient of the nonlinear term in the differential equation. This is a nontrivial task for a general perturbation,

but we could analytically solve this in the short wavelength limit. In this limit we found that the nonlinear coefficient had a positive sign. This meant that in the linearly stable case ($b_2 > 0$) it was possible to be nonlinearly unstable if the initial perturbation was large enough. We found the critical amplitude to be proportional to $\sqrt{b_2}$.

A nonlinear numerical MHD simulation fully confirms the analytic result. We have used a numerical simulation of the nonlinear, full, compressible, MHD equations with small dissipation to verify our analytical result. We showed very good agreement between the simulation and the theory for deviations, b_2, from B_c of up to 10%. The numerical results show that in the short wavelength limit the system is nonlinearly unstable. There is some disagreement in the time evolution of the density with the analytical result, but this is possible since the analytic calculation is for an ideal system with no dissipation. We also discussed why a shift in B_c for the linear instability threshold, due to dissipation, is possible at marginal stability and how it is harder to explain why the nonlinear result has an amplitude dependent stability. Furthermore, the dependence is cubic so the mode grows without bound once it is unstable. This is even harder to explain as a resistive effect.

It should be noted that the fully analytic calculation is facilitated by using a very simple form (a constant) for the transverse stabilizing magnetic field. So, while the conclusions seem to be on solid ground, the application of these findings to various systems, to the extent that the transverse B-field of this analysis is very special, must be appropriately qualified. For example, in tokamaks and stellarators, the interchange mode arises on rational surfaces which corresponds to a slab model

with a sheared magnetic field vanishing at $x = 0$. In the solar coronal case, line-tying is an important characteristic absent in our simple case. Nonetheless, the conclusions are sufficiently dissimilar as to indicate further investigation. Thus, for example, a neighboring nonlinear saturated state for the interchange mode was found in Refs. [25, 26] – whereas the corresponding result in our case, for $b_2 < 0$, indicates a robustly growing mode with no nonlinear saturation. Of course, the transverse magnetic field in these papers was a sheared field with a rational surface for the unstable wave mode. Attempting a marginal stability analysis for sheared field, similar to that used in this analysis, is not straightforward. The fact that the sheared field goes to zero as x goes to zero means that a new inner ordering is required, which makes the calculation more involved.

Our results are more consistent with the nonlinear instability found in Ref. [11] where the authors were also in the parameter range with $k_\perp \gg 1$, $\Delta_x \sim k_\perp^{-1/2}$, and $\xi_x \ll \Delta_x$. It should be noted that their analysis was for the three-dimensional line-tied g mode with no transverse field at marginal stability. Even so, the suprising result is that in both cases the system takes off once it becomes nonlinearly unstable. This occurs even when the linear term is stabilizing. The primary difference between the results is the amplitude dependence of the nonlinear term. In Ref. [11] the nonlinear term has a quadratic dependence, while our analysis yields a cubic dependence on amplitude. If we construct an effective potential, we observe that the result from Ref. [11] indicates a dependence on the sign of the perturbation at the metastable boundary, while our potential is symmetric in A. Another difference is that the result in Ref. [11] was somewhat mitigated by Refs. [27, 28] in that the

latter papers argued that the ordering giving nonlinear growth would break down at small amplitudes before the instability fully takes off. In our case, our numerical simulations seem to show, in agreement with analytic constraints, that the nonlinear instability growth continues without bound and the theory only fails when $A \sim \mathcal{O}(1)$ (as saturation is reached).

Our results could also be relevant to tokamak ballooning modes to the extent that these modes are stabilized by an "average minimum-B well" and thus always have some parallel wavenumber. Work is in progress to quantify this better. Finally, our results also indicate a closer look at interchange stability in stellarators, presumably in average minimum-B stabilized systems.

Further investigation is necessary to answer some questions regarding the results found. The transient initial growth in the time traces, mentioned in Sec. 3.3, needs to be explained. The change in the growth rate as the system gets closer to marginal stability, with $b_2 < 0$, needs to be investigated and compared to the results from Ref. [23]. However, since the natural extension to this analysis is to include variations in z we will continue our investigation with that analysis. The analysis in the next chapter will attempt to resolve the line-tied boundary stabilization established by Refs. [11, 27, 28].

Chapter 4

Three-Dimensional Nonlinear Instability

4.1 Introduction

In the previous chapter, we showed that the two-dimensional (2D) interchange mode near marginal stability can exhibit nonlinearly unstable behaviour. The analysis was done using reduced equations where the parallel wavenumbers were disallowed, i.e. $\partial/\partial z = 0$, and the growth of the interchange was marginally stabilized by a weak B-field transverse to the mode symmetry. In that simplified, 2D system we found that if the initial perturbation was large enough then it would continue to grow without bound, even when the system was linearly stable to interchanges. In this chapter, we extend the analysis to a three-dimensional (3D) system, where stabilization is achieved by allowing for finite wavelength in the z direction.

We consider two boundary conditions in the z direction: periodic and line-tied. The line-tied boundary condition for the interchange mode is a variant of the ballooning instability but with simpler geometry.[27] This is relevant to us since the ballooning mode is a type of interchange mode that can develop in tokamaks, in the regions with curvature unfavorable to the interchange instability.[2] The simpler geometry of the line-tied interchange mode allows us to analyze the nonlinear instabilities that might otherwise not be doable on the complicated geometry of the ballooning mode. We can use this simpler geometry to gain some insight on the

stability of the ballooning mode. In order to bridge the gap from the 2D analysis to a 3D system, we start by considering periodic boundary conditions.

The nonlinear instability result found in the previous chapter is similar to the instability found by Cowley, et al for the line-tied g mode.[11] In that paper, the authors found that the nonlinear line-tied g mode had a regime where the growth became singular at a finite time. Since the nonlinear growth is associated with a release of energy in finite time, the "explosive" growth has been used to explain the onset of magnetospheric substorms[33] and disruptions in tokamak plasmas[34]. Our previous analysis was done in 2D and, therefore, an effective comparison can only be established by extending the method to a 3D system with similar boundary conditions. The goal is to reconcile the differences in our result and the results of Refs. [11] and [27].

In this chapter also, we will do the analysis using slab geometry with an effective gravitational force to model the effects of field line curvature.[15] We begin the analysis by explaining the marginal stability assumption for a 3D system in Sec. 4.2. We then revisit the 2D system with a constant density gradient assumption in Sec. 4.3. In Sec. 4.4 we extend the analysis to a 3D system. Finally, the results are summarized in Sec. 4.5.

4.2 Marginally Stable System

In the analysis that follows, we will once again use the reduced MHD equations, however, we now wish to include variations in z, so the full equations are needed,

which we show here for convenience:

$$\partial_t \rho + \{\varphi, \rho\} = 0, \tag{4.1}$$

$$\hat{\mathbf{z}} \cdot \nabla_\perp \times \rho(\partial_t \mathbf{u} + \{\varphi, \mathbf{u}\}) = B_z \partial_z \nabla_\perp^2 \psi + \{\psi, \nabla_\perp^2 \psi\} + g \partial_y \rho, \tag{4.2}$$

$$\partial_t \psi - B_z \partial_z \varphi - \{\psi, \varphi\} = 0, \tag{4.3}$$

$$\mathbf{u} \equiv \hat{\mathbf{z}} \times \nabla_\perp \varphi, \tag{4.4}$$

$$\mathbf{B} \equiv B_z \hat{\mathbf{z}} + \hat{\mathbf{z}} \times \nabla_\perp \psi, \tag{4.5}$$

where B_z is a constant, g is the magnitude of a constant force in the x direction, and the curly braces denote a Poisson bracket,

$$\{f, h\} \equiv \partial_x f \partial_y h - \partial_y f \partial_x h. \tag{4.6}$$

Since B_z is a constant, these equations describe the nonlinear evolution of the density, ρ, the perpendicular flow, derived from φ, and the perpendicular field, derived from the magnetic flux ψ.

Suppose we have a static equilibrium with a constant density gradient, ρ_0', opposite the gravitational force, and a constant magnetic field, $\mathbf{B_0}$, in the y and z direction. We perturb about this equilibrium by letting

$$\rho = \rho_0 + \tilde{\rho}, \qquad \psi = \psi_0 + \tilde{\psi}, \qquad \text{and} \qquad \varphi = \tilde{\varphi}, \tag{4.7}$$

where the variables with a tilde are a factor of $\epsilon \ll 1$ smaller than the equilibrium quantities. This yields the set of nonlinear equations,

$$\partial_t \tilde{\rho} = \rho_0' \partial_y \tilde{\varphi} + \{\tilde{\rho}, \tilde{\varphi}\}, \tag{4.8}$$

$$\partial_t \tilde{\psi} = \mathbf{B}_0 \cdot \nabla \tilde{\varphi} + \{\tilde{\psi}, \tilde{\varphi}\}, \tag{4.9}$$

$$\partial_t (\rho_0' \partial_x \tilde{\varphi} + \rho_0 \nabla_\perp^2 \tilde{\varphi}) = \mathbf{B}_0 \cdot \nabla \nabla_\perp^2 \tilde{\psi} + g \partial_y \tilde{\rho} + \mathcal{O}(\epsilon^2), \tag{4.10}$$

for the perturbed quantities $\tilde{\rho}$, $\tilde{\psi}$, and $\tilde{\varphi}$. For our analysis, we will consider periodic boundary conditions in the y direction and hard, conducting boundaries in the x direction, i.e. $\tilde{\rho}, \tilde{\psi}, \tilde{\varphi} = 0$ at $x = 0, L_x$. As mentioned earlier, for the 3D problem, we will consider both periodic and line-tied boundary conditions in the z direction.

The boundary conditions and constant ρ_0' allows us to Fourier transform all three directions without having to take the short wavelength and local limits. If we assume small perturbations, so that we can ignore the nonlinear terms, then we get the linear dispersion relation

$$\omega^2 = (\mathbf{k} \cdot \mathbf{V_A})^2 - \gamma_g^2 \frac{k_y^2}{k_x^2 + k_y^2} \tag{4.11}$$

where $\gamma_g^2 = g\rho_0'/\rho_0$ is the Rayleigh-Taylor growth rate driving the instability and $\mathbf{k} \cdot \mathbf{V_A}$ is the frequency of the Alfvénic restoring force due to the equilibrium field. In the short wavelength limit, Eq. (4.11) matches the linear result found in Chapter 2. For $\omega^2 > 0$ field line bending provides enough magnetic tension to stabilize the linear growth of the interchange mode. Similar to the 2D system in the previous chapter we study the dynamics of a marginally stable system, i.e. $\omega^2 \approx 0$, so that

$$\partial_t / \gamma_g \sim \epsilon. \tag{4.12}$$

Equation (4.11) implies that deviations, in $\mathbf{B_0}$, away from the critical field $\mathbf{B_c}$ where

$$(\mathbf{k} \cdot \mathbf{V_{Ac}})^2 - \gamma_g^2 \frac{k_y^2}{k_x^2 + k_y^2} = 0, \tag{4.13}$$

must be of $\mathcal{O}(\epsilon^2)$.

In order to investigate the nonlinear dynamics at marginal conditions, we once again expand the perturbed quantities in a series. For optimal ordering, we scale each successive term smaller by a factor of ϵ. More explicitly, we let

$$\tilde{\rho} = \rho_1 + \rho_2 + \rho_3 + \cdots , \tag{4.14}$$

$$\tilde{\psi} = \psi_1 + \psi_2 + \psi_3 + \cdots , \tag{4.15}$$

$$\tilde{\varphi} = \varphi_1 + \varphi_2 + \varphi_3 + \cdots , \tag{4.16}$$

where the subscript denotes order in ϵ, e.g. $\rho_1/\rho_0 \sim \epsilon$. Furthermore, we again allow for deviations from marginality in the equilibrium field by letting

$$\mathbf{B_0} = \mathbf{B_c} + \mathbf{b_2}, \tag{4.17}$$

where $|\mathbf{b_2}|/|\mathbf{B_c}| \sim \epsilon^2$.

4.3 Two-Dimensional System Revisited: $\partial_z \to 0, \mathbf{B_0} = B_0\hat{\mathbf{y}}$

We start by showing that we recover the nonlinear instability result in the previous chapter for a system with constant density gradient, i.e. $\rho_0'' = 0$. The mathematical method and technique will be similar, so we will be brief on the details. In 2D, Eqs. (4.8) and (4.9) are related by letting

$$\tilde{\rho} = \frac{\rho_0'}{B_0}\tilde{\psi}, \tag{4.18}$$

so we can eliminate $\tilde{\rho}$ as a variable by substituting Eq. (4.18) into Eq. (4.10). By solving for Eqs. (4.9) and (4.10) order by order, we can also satisfy Eq. (4.8).

Matching terms in Eqs. (4.9) and (4.10) to first order in ϵ we get

$$B_c \partial_y \varphi_1 = 0, \tag{4.19}$$

$$\mathcal{L}_{2D}(\psi_1) \equiv (B_c^2 \nabla_\perp^2 + g\rho_0')\partial_y \psi_1 \tag{4.20}$$

$$= 0. \tag{4.21}$$

Therefore, we have a quasistatic, neighboring equilibrium solution

$$\varphi_1 = 0, \tag{4.22}$$

$$\psi_1 = A(t)\sin(k_x x)\cos(k_y y), \tag{4.23}$$

where the phases are chosen to take into account the boundary conditions. Substituting this solution into Eq. (4.21) yields the equation

$$B_c^2(k_x^2 + k_y^2) = g\rho_0', \tag{4.24}$$

for the critical field in the zero frequency mode, given $\mathbf{k}$, g, and ρ_0'. This result is consistent with our assumption in Eq. (4.13).

To second order in ϵ we obtain

$$\partial_t \psi_1 = B_c \partial_y \varphi_2, \tag{4.25}$$

$$\mathcal{L}_{2D}(\psi_2) = 0. \tag{4.26}$$

Equation (4.25) yields a relationship between the lowest order flow, φ_2, and the lowest order flux, ψ_1. From Eq. (4.26) we find that there is only an averaged field to second order, i.e.

$$\psi_2 = \bar{\psi}_2(t, x). \tag{4.27}$$

In order to solve for $\bar{\psi}_2$, and $A(t)$, it is necessary to take Eqs. (4.9) and (4.10) up to third order in ϵ.

So, to third order in ϵ we get

$$\partial_t \psi_2 = B_c \partial_y \varphi_3 + \{\psi_1, \varphi_2\}, \tag{4.28}$$

$$\begin{aligned} \partial_t(\rho_0' \partial_x \varphi_2 \quad + \rho_0 \nabla_\perp^2 \varphi_2) = \tfrac{1}{B_c} \mathcal{L}_{2D}(\psi_3) + 2b_2 \nabla_\perp^2 \partial_y \psi_1 \\ + \{\psi_1, \nabla_\perp^2 \psi_2\} + \{\psi_2, \nabla_\perp^2 \psi_1\}. \end{aligned} \tag{4.29}$$

In writing Eq. (4.29) we take into account corrections to Eq. (4.18) due to b_2, i.e.

$$\rho_3 = \frac{\rho_0'}{B_c}(\psi_3 - \frac{b_2}{B_c}\psi_1), \tag{4.30}$$

and we used Eq. (4.21) to combine the terms proportional to b_2. Averaging Eq. (4.28) in y and simplifying gives us an equation for $\bar{\psi}_2$ in terms of ψ_1,

$$\bar{\psi}_2 = \frac{1}{2}\frac{1}{B_c}\overline{\partial_x(\psi_1^2)} \tag{4.31}$$

$$= \frac{1}{4}\frac{k_x}{B_c} A^2 \sin(2k_x x). \tag{4.32}$$

To simplify Eq. (4.29) we first resolve the Poisson brackets by using Eqs. (4.23) and (4.32) then apply ∂_y to get

$$\begin{aligned} \partial_t^2(\rho_0' \partial_x \psi_1 - \rho_0(k_x^2 + k_y^2)\psi_1) = \mathcal{L}_{2D}(\partial_y \psi_3) \\ + 2b_2 B_c k_y^2 (k_x^2 + k_y^2)\psi_1 + B_c k_y^2 (k_y^2 - 3k_x^2)\partial_x \bar{\psi}_2 \psi_1, \end{aligned} \tag{4.33}$$

where we used Eqs. (4.23) and (4.32) to simplify the second derivatives.

Equation (4.33) is now in the form where we can get a time evolution equation for the amplitude $A(t)$. To do this, we annihilate ψ_3 by projecting the equation onto

ψ_1, using the operator $\int dx \int dy\, \psi_1$, and using integration by parts. The projection yields the time evolution equation

$$\frac{1}{k_y^2 V_{Ac}^2}\frac{d^2}{dt^2}A = -2\frac{b_2}{B_c}A + \frac{1}{4}\frac{k_y^2 - 3k_x^2}{k_x^2 + k_y^2}\frac{A^3}{B_c^2/k_x^2}. \tag{4.34}$$

In the limit where $k_y \gg k_x$ we find that the system is still nonlinearly unstable even with the simplification of taking the density gradient to be constant. This constitutes our motivation to assume constant ρ_0' for the 3D case. We now extend our analysis to a 3D system where we allow for ∂_z variations.

4.4 Three-Dimensional System: $\partial_z \neq 0, \mathbf{B_0} = B_0\hat{\mathbf{z}}$

Consider the magnetic configuration of the 2D case in the y-z plane, shown in Fig. 4.1a. If we have periodic boundary conditions in the z direction then the 2D case can be considered to be a 3D system with a weakly transverse magnetic field but with a perturbation that is a purely perpendicular mode, i.e. $B_y/B_z \ll 1$ and $k_z = 0$. So now consider a straight magnetic field with a weakly transverse perturbation, as shown in Fig. 4.1b. It's easy to see that there should be an isomorphism between this 3D periodic system and the 2D case if $\mathbf{k}\cdot\mathbf{B_0}$ is the same in both cases. This isomorphism can be realized by a change of coordinates where

$$\frac{\partial_z}{k_z} \rightarrow \frac{\partial_y}{k_y}. \tag{4.35}$$

Substituting the above into Eqs. (4.8)-(4.10) we find that the equations are the same as the ones used in Sec. 4.3 if we let

$$B_{y0} = \frac{k_z}{k_y}B_{z0}, \tag{4.36}$$

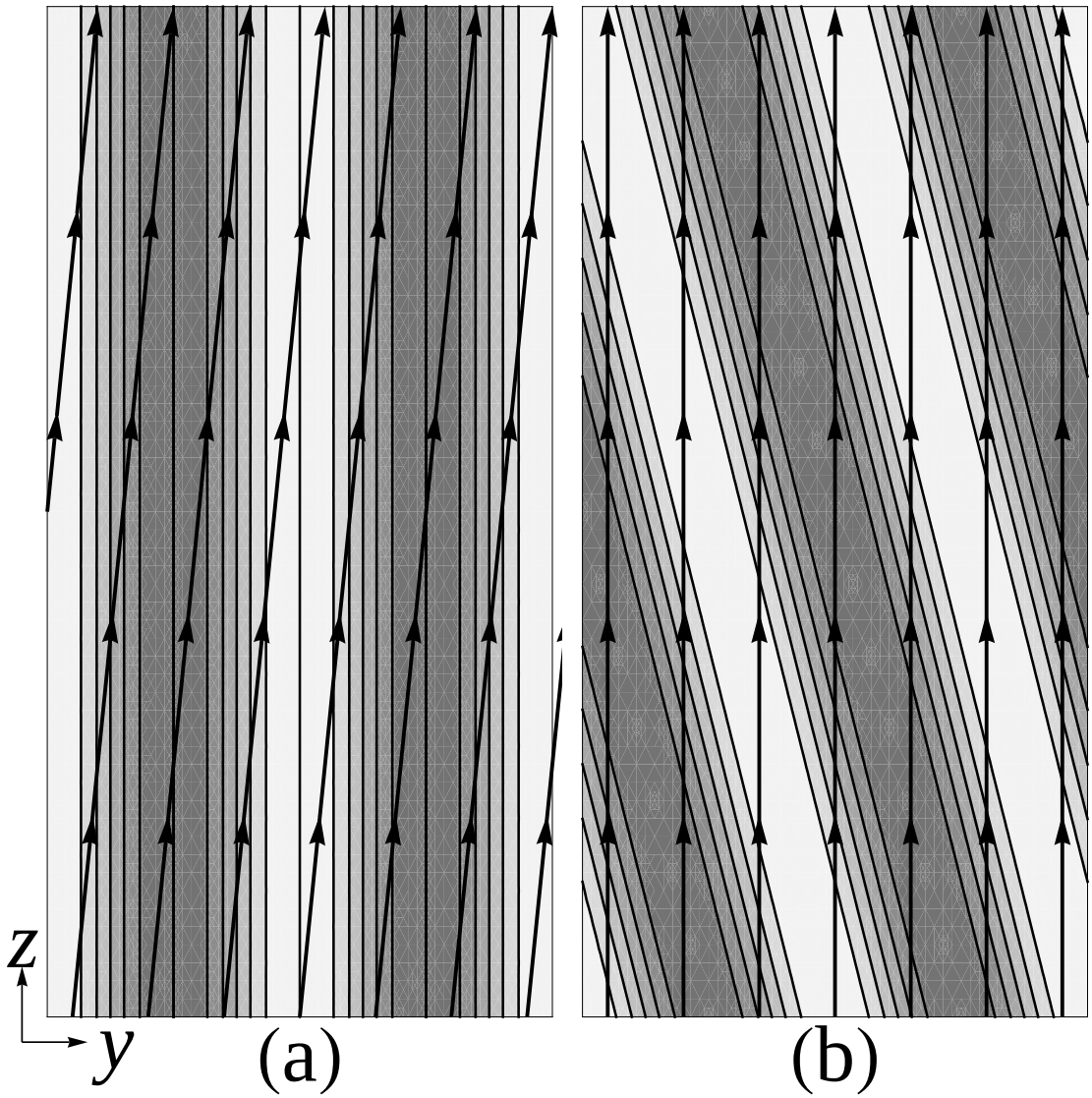

Figure 4.1: Cartoon of the equilibrium magnetic field lines and contours of the first order density perturbation for: (a) 2D problem with $k_z = 0$, $B_y \neq 0$ and (b) isomorphic 3D problem with $k_z \neq 0$, $B_y = 0$.

which is the expected condition to have an isomorphism. So, this means that the isomorphic problem yields the nonlinear time evolution equation

$$\frac{1}{k_z^2 V_{Ac}^2}\frac{d^2}{dt^2}A = -2\frac{b_2}{B_c}A + \frac{1}{4}\frac{k_y^2 - 3k_x^2}{k_x^2 + k_y^2}\frac{k_y^2}{k_z^2}\frac{A^3}{B_c^2/k_x^2}, \tag{4.37}$$

which is just Eq. (4.34) but substituting Eq. (4.36).

Equation (4.37) can be arrived at, more explicitly, by using the solution

$$\psi_1 = A(t)\sin(k_x x)\cos(k_y y + k_z z) \tag{4.38}$$

and following a similar process as in the 2D case. However, since this problem is fully 3D, Eq. (4.18) is no longer a valid substitution and, thus, it is necessary to solve Eqs. (4.8)-(4.10) simultaneously order by order. This explicit calculation is shown in Appendix C.

The periodic solution given in Eq. (4.38) is a linear combination of modes where the y and z dependences are decoupled from each other. These modes, shown in Fig. 4.2a, have a "blob"-like structure and, depending on the phase and wavenumber of the solution, can be applied to a system with line-tied boundary conditions, as in Fig. 4.2b. Because of this similarity we can treat both of these problems at the same time. We will use the same approach as in the 2D case and solve Eqs. (4.8)-(4.10) order by order by matching terms in powers of ϵ.

To first order in ϵ, Eqs. (4.8) and (4.9) give

$$\rho_0'\partial_y\varphi_1 = 0, \tag{4.39}$$

$$B_c\partial_z\varphi_1 = 0. \tag{4.40}$$

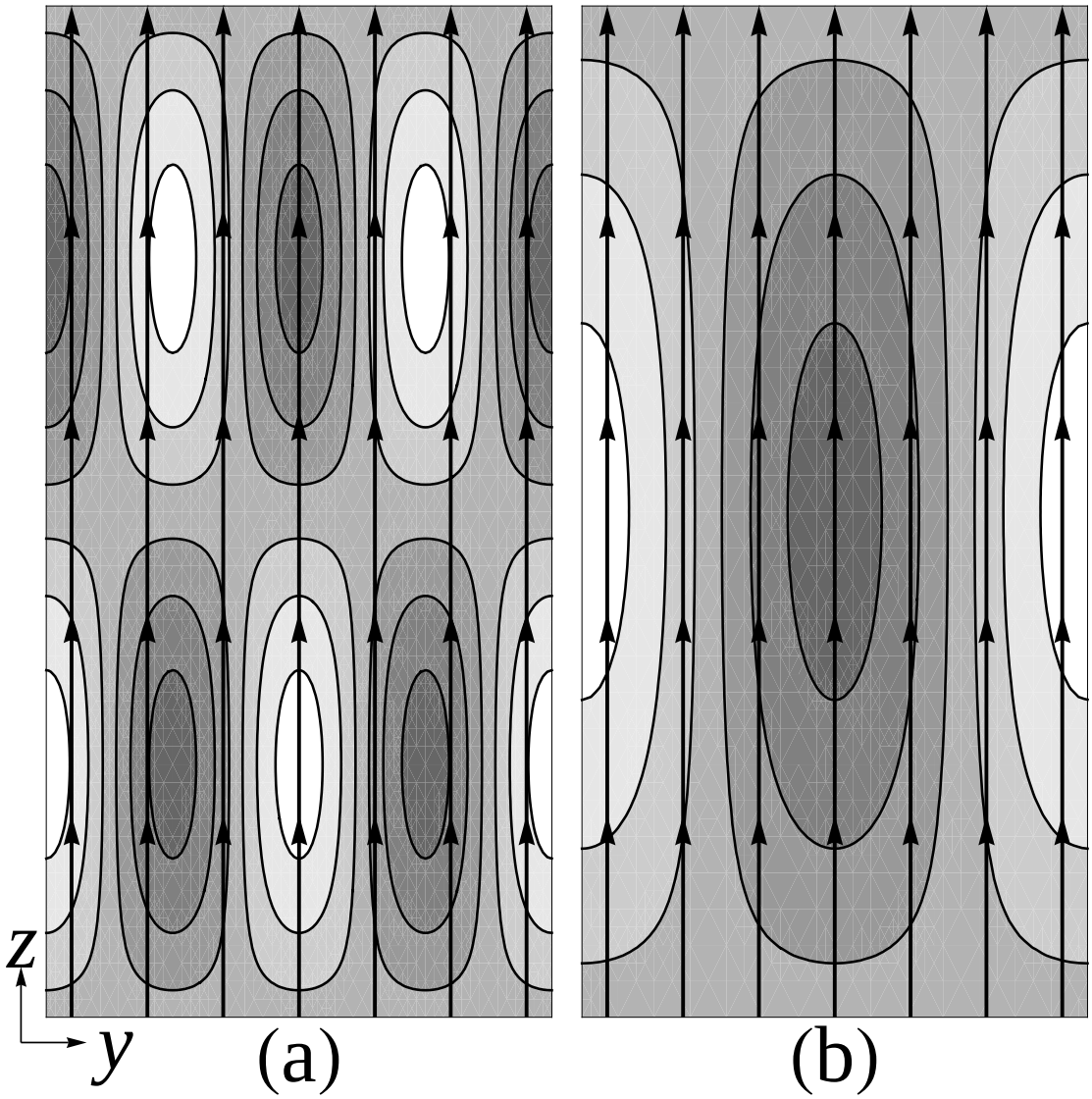

Figure 4.2: Cartoon of the equilibrium magnetic field lines and contours of the first order density perturbation for a 3D problem with (a) periodic and (b) line-tied boundary conditions in the z direction.

We take the solution to be quasistatic with $\varphi_1 = 0$, which means that we have to rescale the flow to be of at least order ϵ^2. So, to lowest significant order we now get

$$\partial_t \rho_1 = \rho_0' \partial_y \varphi_2, \tag{4.41}$$

$$\partial_t \psi_1 = B_c \partial_z \varphi_2, \tag{4.42}$$

$$B_c \partial_z \nabla_\perp^2 \psi_1 + g \partial_y \rho_1 = 0. \tag{4.43}$$

Taking ∂_t of Eq. (4.43) and substituting for ρ_1 and ψ_1 we get

$$\mathcal{L}_{3D}(\varphi_2) \equiv (B_c^2 \partial_z^2 \nabla_\perp^2 + g\rho_0' \partial_y^2)\varphi_2 \tag{4.44}$$

$$= 0, \tag{4.45}$$

which is an eigenvalue problem for φ_2 and B_c, and is the 3D counterpart to Eq. (4.21). As mentioned earlier, we are interested in solutions where the y and z dependence are decoupled from each other. We write the solution of Eq. (4.45) in the form

$$\varphi_2 = \frac{1}{k_z B_c} \dot{A}(t) \sin(k_z z) \zeta(x, y) \tag{4.46}$$

where

$$\zeta(x, y) = \sin(k_x x) \cos(k_y y). \tag{4.47}$$

Substituting this solution into Eqs. (4.41) and (4.42) gives the rest of the lowest order solutions

$$\rho_1 = \frac{\rho_0'}{k_z B_c} A(t) \sin(k_z z) \partial_y \zeta(x, y), \tag{4.48}$$

$$\psi_1 = A(t) \cos(k_z z) \zeta(x, y), \tag{4.49}$$

and substituting into Eq. (4.45) yields the equation

$$B_c^2 k_z^2 (k_x^2 + k_y^2) = g \rho_0' k_y^2, \tag{4.50}$$

for B_c given g, ρ_0' and $\mathbf{k}$.

Matching terms to next significant order yields

$$\partial_t \rho_2 = \rho_0' \partial_y \varphi_3 + \{\rho_1, \varphi_2\}, \tag{4.51}$$

$$\partial_t \psi_2 = B_c \partial_z \varphi_3 + \{\psi_1, \varphi_2\}, \tag{4.52}$$

$$B_c \partial_z \nabla_\perp^2 \psi_2 + g \partial_y \rho_2 + \{\psi_1, \nabla_\perp^2 \psi_1\} = 0. \tag{4.53}$$

Using Eqs. (4.46)-(4.49) to simplify the Poisson brackets, we find that

$$\{\psi_1, \varphi_2\} \propto \{\zeta, \zeta\} \tag{4.54}$$

$$= 0, \tag{4.55}$$

$$\{\psi_1, \nabla_\perp^2 \psi_1\} \propto -(k_x^2 + k_y^2)\{\zeta, \zeta\} \tag{4.56}$$

$$= 0. \tag{4.57}$$

After taking the ∂_t of Eq. (4.53) and substituting for ρ_2 and ψ_2 using Eqs. (4.51) and (4.52) we obtain a simple equation for φ_3

$$\mathcal{L}_{3D}(\varphi_3) = 0, \tag{4.58}$$

since

$$\partial_y\{\rho_1, \varphi_2\} \propto \partial_y\{\partial_y\zeta, \zeta\} \tag{4.59}$$

$$= \{\partial_y\zeta, \partial_y\zeta\} + \{\partial_y^2\zeta, \zeta\} \tag{4.60}$$

$$= -k_y^2\{\zeta, \zeta\} \tag{4.61}$$

$$= 0. \tag{4.62}$$

There are a family of solutions that satisfy Eq. (4.58) and (4.50). Of these solutions, we can take the simplest one with

$$\varphi_3 = 0, \tag{4.63}$$

without loss of generality. The nonzero solutions do not contribute to the time evolution equation since the projection method to annihilate φ_4, applied to these terms, evaluates to zero. This is due to the fact that the z dependence of the solutions has to be the same mode number as the lowest order solutions, i.e. $\varphi_3 \sim \sin(k_z z)$ or $\cos(k_z z)$, and only the zeroth and second order harmonics of the second order solutions contribute to the final equation. Equation (4.63) then implies that

$$\rho_2 = \frac{1}{4}\frac{\rho_0'}{B_c^2}\frac{k_y^2}{k_z^2}k_x A^2 \sin(k_z z)^2 \sin(2k_x x), \tag{4.64}$$

$$\psi_2 = 0, \tag{4.65}$$

are the solutions to the second order perturbation.

Carrying on with the analysis, we take Eqs. (4.8) and (4.9) to fourth order in ϵ,

$$\partial_t \rho_3 = \rho_0' \partial_y \varphi_4 + \{\rho_2, \varphi_2\}, \tag{4.66}$$

$$\partial_t \psi_3 = B_c \partial_z \varphi_4 + b_2 \partial_z \varphi_2, \tag{4.67}$$

and Eq. (4.10) to third order,

$$\partial_t(\rho_0' \partial_x \varphi_2 + \rho_0 \nabla_\perp^2 \varphi_2) = B_c \partial_z \nabla_\perp^2 \psi_3 + g \partial_y \rho_3 + b_2 \partial_z \nabla_\perp^2 \psi_1. \tag{4.68}$$

We can combine all three equations by once again taking ∂_t of Eq. (4.68) and substituting for ρ_3 and ψ_3 using Eqs. (4.66) and (4.67). After simplification, this sub-

stitution yields

$$\partial_t^2(\rho_0'\partial_x\varphi_2 - (k_x^2+k_y^2)\rho_0\varphi_2) = \mathcal{L}_{3D}(\varphi_4) + 2b_2B_ck_z^2(k_x^2+k_y^2)\varphi_2 - gk_y^2\partial_x\rho_2\varphi_2, \tag{4.69}$$

where we made use of the fact that ρ_2 does not depend on y to get the last term.

We are now ready to apply an annihilator to eliminate φ_4 and arrive at a time evolution equation for $A(t)$. Projecting Eq. (4.69) onto φ_2 by applying $\int dx \int dy \int dz\, \varphi_2$ to the equation results in

$$\frac{1}{k_z^2V_{Ac}^2}\frac{d^2}{dt^2}A = -2\frac{b_2}{B_c}A - \frac{1}{16}\frac{k_y^2}{k_z^2}\frac{A^3}{B_c^2/k_x^2} \tag{4.70}$$

as the nonlinear time evolution equation for the 3D interchange problem with decoupled initial conditions.

Comparing Eqs. (4.37) and (4.70), we can see that the nonlinear term in the blob-like modes differ from the isomorphic mode, in the large k_y limit. This implies that the nonlinear stability of the 3D interchange mode problem is dependent on the choice of the initial state of the perturbation. The isomorphic problem with perturbation given by Eq. (4.38), and mode structure shown in Fig. 4.1b, yields the expected nonlinear instability found in the previous chapter for the 2D case. However, perturbations of the form given by Eq. (4.49), and mode structure shown in Fig. 4.2, have maximum amplitudes that can saturate over time. Since k_z is not specified in the problem, we can pick it in such a way that $\tilde{\varphi}$ and $\tilde{\rho}$ are zero at the boundaries on the z direction, i.e. the boundary conditions for a line-tied system. Therefore, our results have shown that the perturbation amplitude of the marginally

stable, line-tied interchange mode is bounded and nonlinear growth is suppressed. In both cases, linear theory predicts that the amplitude will remain bounded with oscillatory solutions when $|\mathbf{B_0}| > |\mathbf{B_c}|$, i.e. $b_2 > 0$. If the system was marginally unstable, i.e. $b_2 < 0$, then the line-tied interchange mode can exhibit some weak nonlinear suppression.

4.5 Summary and Conclusions

In this chapter, we extended the analysis of the nonlinear interchange mode to a 3D system, using the reduced equations. We first showed that we could simplify the system further by assuming that we have a flat density gradient, i.e. ρ_0' constant. Having a constant density gradient meant that the eigenvalue problem for the form factor, i.e. x dependence, of the first order perturbation can be solved for by introducing a wavenumber in the x direction. It was found that, even with this assumption, the simplified calculation still recovers the nonlinear instability result found in the 2D system, thus, this assumption is suitable for the extension of our analysis. We then showed, by considering $\mathbf{B}\cdot\mathbf{k}$, that the 2D system with a transverse magnetic field and no ∂_z variation is isomorphic to a 3D system with only straight field lines and $k_z \neq 0$. This would mean that the 3D system with periodic boundary conditions and initial condition given by Eq. (4.38) would result in the same nonlinear instability for large enough initial perturbations. The only difference is that the linear term is now proportional to $k_z B_z$, instead of $k_y B_y$, and the nonlinear term has a dependence on the ratio k_y/k_z. Finally, we showed that the y and z dependence

can be decoupled to create a different set of initial conditions with blob-like mode structure similar to ballooning modes. With the appropriate choice of wavenumber, these modes can satisfy periodic or line-tied boundary conditions. It was found that the nonlinear term of these modes had the opposite sign compared to the 2D and isomorphic modes, which implies that these modes are nonlinearly stable when close to marginal conditions.

The result of the nonlinear analysis for the line-tied interchange mode system is similar to the ones found in Ref. [27] for the line-tied g mode. In the paper, the authors also found that when revisiting the result of Cowley, et al in Ref. [11] they were only able to recover the nonlinear instability in the line-tied g mode in the regime where the perturbations remained small (what they refer to as the "Cowley-Artun regime"). When the perturbation is sufficiently large they find that there exists an "intermediate regime" that alters the nonlinear behaviour and suppresses the nonlinear growth. They conclude that the latter phase is the more relevant nonlinear result since it is realized in a larger set of initial conditions than the Cowley-Artun regime.[28]

Even though the findings are similar, the mechanisms that controls the nonlinear mode growth are different. Zhu, et al found that, when transitioning between the two regimes, compressibility starts becoming much more important.[28] Since our analysis was done using the reduced equations, incompressibility is inherently assumed and, thus, cannot appear in the analysis without starting with the full MHD equations. We can determine the cause of the nonlinear instability in the isomorphic system by comparing the calculations in Appendix C and Sec. 4.4. Comparing the

second order solutions for the magnetic flux (Eqs. (4.65) and (C.19)) we can see that the isomorphic modes generate an averaged flux unlike the blob-like modes. This term is what drives the nonlinear instability.

The analysis presented in this chapter was completed using a simple model system so it does not contain the details of a more realistic ballooning mode system. However, the result is in very close agreement to the ones found by Zhu, et al in their more comprehensive analysis of the line-tied g mode. Additionally, nonlinear simulations of a more realistic system have found similar results to the ones found in this chapter.[28, 35] This is remarkable in that, comparatively, our methodology is much more simple than the ones carried out by Refs. [11] and [27].

It is possible to apply our method using the full MHD equations to gain some insight in the question of compressibility, but it is unclear how much more insight we can gain from doing this. It is more fruitful to apply the analysis to a different question regarding stability. Up to now we have been using an initial perturbation that affects the system globally and attempting to determine the time evolution of this perturbation. However, one can also ask the question of what happens if we have a local perturbation. For instance, what happens if the boundary of the system was perturbed? In the next chapter, we will apply our method to try and answer this question.

Chapter 5

Boundary Induced Instability

5.1 Introduction

As has been discussed, magnetically confined plasmas for fusion are limited in how much pressure can be contained, by the so-called β limit – the critical ratio of pressure to magnetic energy density.[2] This limitation generally comes from interchange instabilities, wherein flux tubes of high pressure plasma can interchange with outer, lower pressure flux tubes.[2, 15, 17] Such energy release can be stabilized if the flux tube interchange is disallowed by topology (on account of the frozen-in condition for strongly magnetized plasmas), that is to say, if the "transverse" field is strong enough.[15] For maximum efficiency, one wants to operate close to marginal stability, $\beta \to \beta_c$.

In this chapter, we look into two different results pertaining to operating near marginal stability. Let $\Delta\beta = \beta_c - \beta$ and let the system size be a. Then, (1) we establish the general idea that a small perturbation of δ/a on the boundary *amplifies* interchange displacements in the core of the plasma, by an amplification factor $\beta_c/\Delta\beta$; (2) we show that the system is *nonlinearly unstable*, so that a critical boundary perturbation will destabilize the interchange mode even for systems below the linear β stability limit. Upon combining these two findings, we find that the amplification phenomenon leads to a nonlinear instability criterion which is highly sensitive

to boundary perturbations, namely the fractional critical size is even smaller than the fractional deviation from marginality, i.e., $(\delta/a) > |\Delta\beta/\beta_c|^{3/2}$. This has the implication that magnetic configurations designed to confine plasma close to the β limit within a tolerance of ϵ would necessitate that the design be more sensitive to boundary perturbations; specifically, boundary tolerances need to be better than $\epsilon^{3/2}$. Such considerations are of significant importance in the design of axisymmetric tolerances for advanced tokamaks as well as in the fully 3D design of stellarators for fusion.

Field amplification near marginal stability has been shown to also occur in tokamak plasmas, for kinklike[36] and tearing[37, 38] modes. It was reported in Ref. [37] that external perturbations would be amplified if the equilibrium profile is close to marginal stability for tearing. In Refs. [36, 38], it was shown that error fields at the plasma edge are amplified in the core by a factor that is inversely proportional to the marginal stability parameter. It has also been shown that the effect of plasma response in the bulk could be important in explaining the effects of boundary perturbations.[39] Our present result shows that the amplification phenomenon extends also to interchange modes (as also found in a related case in Ref. [12]). We include nonlinear perturbations in our methodology to show that the amplification precipitates an already dormant nonlinear instability.

We again use a model system to illustrate the basic phenomena. The calculation is done in slab geometry with an effective gravitational field to model field line curvature. Boundary perturbations are treated as a ripple on the boundary conditions, similar to the Kulsrud-Hahm problem.[40]

5.2 Linear Boundary Perturbation Problem

We begin with a simple-minded linear calculation to first demonstrate the amplification phenomenon. Consider an incompressible system describable by the two-dimensional, reduced MHD equations, rewritten here:

$$\partial_t \psi = \{\psi, \varphi\}, \tag{5.1}$$

$$\hat{\mathbf{z}}\cdot\nabla_\perp\times\rho(\partial_t\mathbf{u} + \{\varphi, \mathbf{u}\}) = \{\psi, \nabla_\perp^2\psi\} + g\partial_y\rho, \tag{5.2}$$

$$\mathbf{u} = \hat{\mathbf{z}}\times\nabla_\perp\varphi, \quad \mathbf{B}_\perp = \hat{\mathbf{z}}\times\nabla_\perp\psi, \tag{5.3}$$

where, in general, $\rho = \rho(\psi)$ and the curly braces are a Poisson bracket defined by,

$$\{f, h\} \equiv \partial_x f\partial_y h - \partial_y f\partial_x h. \tag{5.4}$$

The problem of interest is illustrated in Fig. 5.1 with ρ_0' and B_0 constant, and such that we are stable to the ideal MHD interchange mode. The system is taken to be periodic in the y direction, and

$$\partial_y\psi = -k\sin(ky)\delta\partial_x\psi \tag{5.5}$$

at $x = \pm a - \delta\cos(ky)$ provides the rippled boundary condition in the x direction. The x boundary condition is derived from insisting that $\mathbf{B}\cdot\hat{\mathbf{n}} = 0$, where $\hat{\mathbf{n}}$ is the direction normal to the surface, since we're assuming conducting plates. For $\delta = 0$ this system is in static equilibrium.

We now perturb the boundaries at $x = \pm a$ by adiabatically introducing $\delta/a \ll 1$ and allowing for a quasistatic equilibrium, $\psi = B_0 x + \tilde{\psi}$, to form. In general, $\tilde{\psi}$

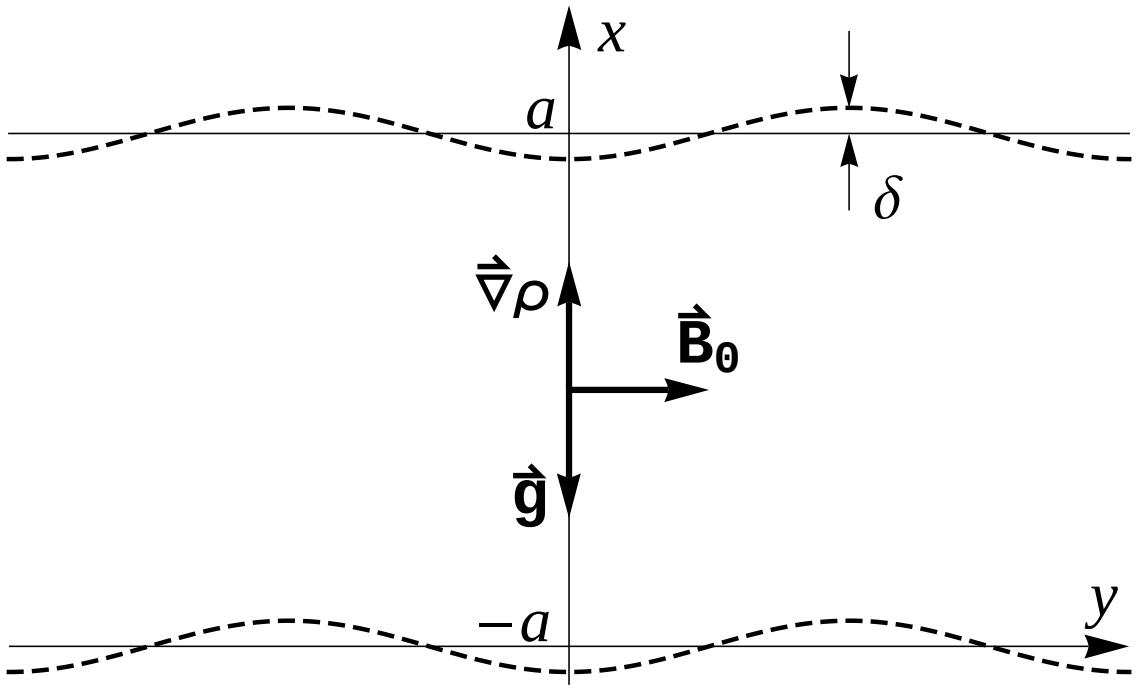

Figure 5.1: The conducting plate boundaries, at $x = \pm a$, of a system with $\vec{\nabla}\rho = \rho_0'\hat{\mathbf{x}}$ opposite a gravitational force $\vec{\mathbf{g}} = -g\hat{\mathbf{x}}$ balanced by a transverse field $\vec{\mathbf{B}}_0 = B_0\hat{\mathbf{y}}$ are perturbed by a ripple of amplitude δ.

satisfies the nonlinear equation

$$(B_0^2\nabla_\perp^2 + g\rho_0')\partial_y\tilde{\psi} = -B_0\{\tilde{\psi}, \nabla_\perp^2\tilde{\psi}\}, \tag{5.6}$$

and the boundary condition, Eq. (5.5). In writing the above equation we made use of the fact that $\rho = \rho(\psi)$ and substituted for $\tilde{\rho}$ using the equation

$$\tilde{\rho} = \frac{\rho_0'}{B_0}\tilde{\psi}. \tag{5.7}$$

The solution

$$\tilde{\psi} = \frac{\delta B_0}{\cos(k_x a)}\cos(k_x x)\cos(ky), \tag{5.8}$$

where

$$k_x^2 = \frac{g\rho_0'}{B_0^2} - k^2, \tag{5.9}$$

satisfies Eq. (5.6) and Eq. (5.5) to lowest (linear) order in δ/a. From Eq. (5.8), we note that as $k_x a$ approaches $\pi/2$, the perturbation gets amplified. In fact, as we will confirm later, $k_x a = \pi/2$ corresponds precisely to the linear stability criterion for the ideal interchange mode, where the critical transverse field for marginal stability, $B_0 = B_c$, is obtained from Eq. (5.9) at $k_x = k_c \equiv \pi/2a$.

We can determine the scaling of this amplification by letting $B_0 = B_c + b$ and $k_x = k_c - \Delta k_x$, where $b/B_c \sim \Delta k_x/k_c \ll 1$. To lowest order in b/B_c

$$\Delta k_x = \frac{b}{B_c}\frac{k_\perp^2}{k_c}, \tag{5.10}$$

where $k_\perp^2 \equiv k_c^2 + k^2$, and Eq. (5.8) yields

$$\tilde{\psi} \approx \frac{\delta/a}{b/B_c}\frac{k_c}{k_\perp^2}B_c\cos(k_x x)\cos(ky). \tag{5.11}$$

Therefore, as we approach criticality by letting $b \to 0$, a small perturbation at the boundary of $\mathcal{O}(\delta/a)$ can induce a large response in the bulk of the plasma, scaling like $B_c\delta/ba$. At exactly $B_0 = B_c$ the solution becomes ill-defined away from the boundary.

From Eq. (5.11) we can also see that the amplification is global, i.e. it occurs everywhere away from the boundary, despite the fact that the perturbation is only on the boundary. This raises an interesting question regarding the penetration depth of the perturbation. What if the the system was only marginal in a narrow region near the origin and was stable, and far from marginal, everywhere else? Putting this in context of the problem, consider the situation with

$$\rho_0'(x) = \rho_0' a\delta(x), \tag{5.12}$$

where $\delta(x)$ is the Dirac delta function (not to be confused with the boundary perturbation). In what conditions, if there are any, is there an amplification?

To lowest order in δ/a we can satisfy Eqs. (5.6) and (5.5), using the density gradient given by Eq. (5.12), by letting $\tilde{\psi} = F(x)\cos(ky)$, where $F(x)$ is the solution to

$$F''(x) = k^2 F(x), \tag{5.13}$$

$$F(\pm a) = B_0\delta, \tag{5.14}$$

and the jump condition

$$2F'(0) = -\frac{g\rho_0'}{B_0^2} aF(0) \tag{5.15}$$

$$\equiv -\kappa^2 aF(0), \tag{5.16}$$

along with the requirement that $F(x)$ be continuous at $x = 0$. From this, we find that

$$F(x) = B_0\delta\frac{ka\cosh(kx) \mp \frac{1}{2}\kappa^2a^2\sinh(kx)}{ka\cosh(ka) - \frac{1}{2}\kappa^2a^2\sinh(ka)}, \tag{5.17}$$

where the minus and plus refer to the $x > 0$ and $x < 0$ solutions, respectively. It is easy to show that, for the case with $\delta = 0$, there exists a nontrivial solution when the following condition

$$ka\cosh(ka) = \frac{1}{2}\kappa^2a^2\sinh(ka) \tag{5.18}$$

is satisfied. Similar to the previous case with amplification as k_xa approached $\pi/2$, when the above critical condition is approached, the solution given by Eq. (5.17) gets amplified. This means that despite only having an extremely narrow region where an instability could occur, amplification from boundary perturbations is still possible in the bulk of the plasma.

The details of the penetration of the boundary perturbations can be established better by considering the short and long wavelength limits. In the limit where $ka \gg 1$, we find that

$$F(x) = 2B_0\delta e^{-ka}\cosh(kx), \tag{5.19}$$

which means that it is not possible to induce this amplification phenomenon. However, in the limit with $ka \ll 1$, we find that

$$F(x) = B_0\delta\frac{1 - \frac{1}{2}\kappa^2a|x|}{1 - \frac{1}{2}\kappa^2a^2}, \tag{5.20}$$

and the system can become amplified. What this implies is that, in the short wavelength limit, the perturbations decay exponentially away from the boundary and

are unable to induce the amplification, but long wavelength perturbations are able to penetrate to the core and induce a global amplification. For a general k and ρ_0', the boundary perturbation will remain flat or decay away from the boundary until it reaches, if possible, the region where amplification is possible. When marginality is approached the amplification can be induced and spread out globally, beyond the initial region, all the way to the boundary.

It should be noted that if we consider $B_c\delta \sim ba$ then ideal MHD is insufficient to describe the amplification phenomena. At $y = 0$

$$\mathbf{B} \approx B_c(1 - \frac{\delta/a}{b/B_c}\frac{k_c^2}{k_\perp^2}\sin(k_x x))\hat{\mathbf{y}}, \tag{5.21}$$

therefore away from the boundary at

$$x = \frac{2a}{\pi}\sin^{-1}(\frac{b/B_c}{\delta/a}\frac{k_\perp^2}{k_c^2}) \tag{5.22}$$

the total magnetic field goes to zero and an X-point is created in the magnetic configuration. This change in magnetic field geometry is not allowed in ideal MHD since it requires a change in magnetic topology.

The analysis with density gradient given by Eq. (5.12) and the solution given by Eq. (5.8) is valid as long as δ/a is small, such that $B_c\delta \ll ba$. However, this clearly establishes the phenomenon of amplification. We show in what follows that nonlinear effects arise at even smaller boundary amplitudes, significantly modifying our understanding of the effect of boundary perturbations on stability. In the following analysis, we will again take ρ_0' to be constant everywhere.

5.3 Nonlinear Evolution

For a system that is marginally stable to the ideal MHD interchange mode, we previously showed in Chapter 3 that small homogeneous perturbations in the plasma can result in nonlinear, explosive growth. The nonlinear instability result showed that the optimal scaling of magnetic perturbations was given as $|\tilde{\psi}/\psi_0| \sim \epsilon \equiv (b/B_c)^{1/2}$. This realization prompts us to apply this nonlinear stability scaling as optimal ordering for nonlinearities in the present amplification calculation. Thus, optimally, we should have $\delta/a \sim \epsilon^3$, using Eq. (5.11). With this scaling, we will show that δ on the boundary can introduce a nonlinear instability in the plasma. It is important to note that even though we order the parameters as described, the boundary perturbation amplitude, δ/a, and marginality condition, b/B_c, are independent, small parameters.

Using the marginality condition as a smallness parameter we expand ψ in a series, i.e. let

$$\psi = \psi_0 + \psi_1 + \psi_2 + \psi_3 + \cdots , \tag{5.23}$$

where each successive term is smaller by a factor of ϵ and $\psi_0 = (B_c + b)x$. By matching terms order by order, we solve Eq. (5.6), where $\tilde{\psi} = \psi - \psi_0$, using the boundary condition given by Eq. (5.5).

To order ϵ, Eq. (5.6) yields

$$B_c^2(\nabla_\perp^2 + k_\perp^2)\partial_y\psi_1 = 0, \tag{5.24}$$

where we have substituted for $g\rho_0'$ using Eq. (5.9) with $B_0 = B_c$ and $k_x = k_c$. Taking

Eq. (5.5) to lowest order implies that

$$\partial_y \psi_1|_{x=\pm a} = 0. \tag{5.25}$$

Including the lowest order (in ϵ) term in the solution given by Eq. (5.8), we find that

$$\psi_1 = \left[A + \frac{\delta/a}{b/B_c} \frac{k_c}{k_\perp^2} B_c \right] \cos(k_c x) \cos(ky), \tag{5.26}$$

where, for convenience, A is introduced as a free parameter in this particular manner to represent the plasma response. We are interested in how δ in the boundary induces A in the plasma. We use the scaling $k_c A/B_c \sim \epsilon$ for the plasma perturbation, but it will be treated as a separate small parameter.

The lowest order equation, given by Eq. (5.24), can also be arrived at by solving the linear, ideal MHD, interchange mode problem and insisting that $\omega = 0$. This results in a zero frequency state, given by Eq. (5.26) with $\delta = 0$, where Alfvénic restoring forces exactly balances the Rayleigh-Taylor growth rate, i.e. $k_\perp^2 V_{Ac}^2 - g\rho_0'/\rho_0 = 0$. From this, we can conclude that B_c is the critical field strength needed to be at marginal conditions. Allowing for $b > 0$ means that the system is marginally stable to the ideal MHD interchange mode. This calculation is similar to the lowest order calculation for the two-dimensional case in the previous chapter, but using an even solution in $|x| \leq a$.

Continuing to order ϵ^2, we find that ψ_2 satisfies the equation

$$B_c^2(\nabla_\perp^2 + k_\perp^2)\partial_y \psi_2 = -B_c\{\psi_1, \nabla_\perp^2 \psi_1\} \tag{5.27}$$

$$= 0 \tag{5.28}$$

and the boundary condition

$$\partial_y \psi_2|_{x=\pm a} = 0. \tag{5.29}$$

This implies that ψ_2 is only a function of x. We can solve for ψ_2 by taking Eq. (5.1) to second order and averaging over y to get

$$\partial_t \psi_2 = \overline{\partial_x(\partial_y \tilde{\varphi} \psi_1)}, \tag{5.30}$$

where the bar denotes an average over y. Equation (5.1) to lowest order implies that

$$\partial_t \psi_1 = B_c \partial_y \tilde{\varphi}, \tag{5.31}$$

and so we find that

$$\psi_2 = -\frac{1}{4}\frac{k_c}{B_c}\left[A + \frac{\delta/a}{b/B_c}\frac{k_c}{k_\perp^2}B_c\right]^2 \sin(2k_c x). \tag{5.32}$$

This term represents the flattening of the perturbed field lines (zonal field) to second order, driven by the first order perturbation. The term also generates quasi-linear flattening of the density profile since the density and flux are related by Eq. (5.7).

In order to find how δ drives the amplitude A we extend our analysis to order ϵ^3 where Eq. (5.6) yields

$$\begin{aligned} B_c^2(\nabla_\perp^2 + k_\perp^2)\partial_y \psi_3 + 2B_c b \nabla_\perp^2 \partial_y \psi_1 = \\ - B_c(\{\psi_1, \nabla_\perp^2 \psi_2\} + \{\psi_2, \nabla_\perp^2 \psi_1\}), \end{aligned} \tag{5.33}$$

with the boundary condition

$$\partial_y \psi_3|_{x=\pm a} = -\delta B_c k \sin(ky). \tag{5.34}$$

The above equations imply that $\psi_3 = \psi_3(x)\cos(ky)$ where $\psi_3(x)$ is a linear combination of k_c and $3k_c$ harmonic terms. The $3k_c$ harmonic is straightforward and uninteresting; however, the k_c harmonic is secular, so we will focus on obviating this secularity. Expanding the solution given by Eq. (5.8) in a series in ϵ yields the third order solution

$$\psi_3 = B_c \frac{\delta}{a} x \sin(k_c x)\cos(ky). \tag{5.35}$$

Substituting Eqs. (5.26), (5.32), and (5.35) into Eq. (5.33) and insisting that the secular terms go to zero yields

$$-2B_c bA + \frac{k_c^2}{4}\frac{k^2 - 3k_c^2}{k_\perp^2}\left[A + \frac{\delta/a}{b/B_c}\frac{k_c}{k_\perp^2}B_c\right]^3 = 0, \tag{5.36}$$

after simplification. The above result gives the sought-after relationship between the boundary perturbation amplitude and the amplitude of the plasma response.

To discuss this result we now consider allowing for the plasma response to evolve in time, at a rate slower than Alfvén time, $\tau_A = (k_c V_{Ac})^{-1}$, as we distort the boundary at an even slower rate. Explicitly, we let $A = A(t)$ with $\tau_A \partial_t \sim \epsilon$ but we keep $\dot{\delta}$ small. It is easy to show that doing this results in the nonlinear time evolution of $A(t)$ given by

$$\frac{1}{k^2}\ddot{A} = -2bA + \frac{1}{4}\frac{k^2 - 3}{k^2 + 1}\left[A + \frac{2}{\pi}\frac{\delta}{b}\frac{1}{k^2 + 1}\right]^3, \tag{5.37}$$

where we normalize the variables by setting k_c, B_c, and V_{Ac} equal to 1, for simplicity. Multiplying Eq. (5.37) by $\dot{A}$ and integrating once yields the "energy" integral $E_0 = \dot{A}^2/2k^2 + U(A;\delta)$, where

$$U(A;\delta) = bA^2 - \frac{1}{16}\frac{k^2 - 3}{k^2 + 1}\left[A + \frac{2}{\pi}\frac{\delta}{b}\frac{1}{k^2 + 1}\right]^4. \tag{5.38}$$

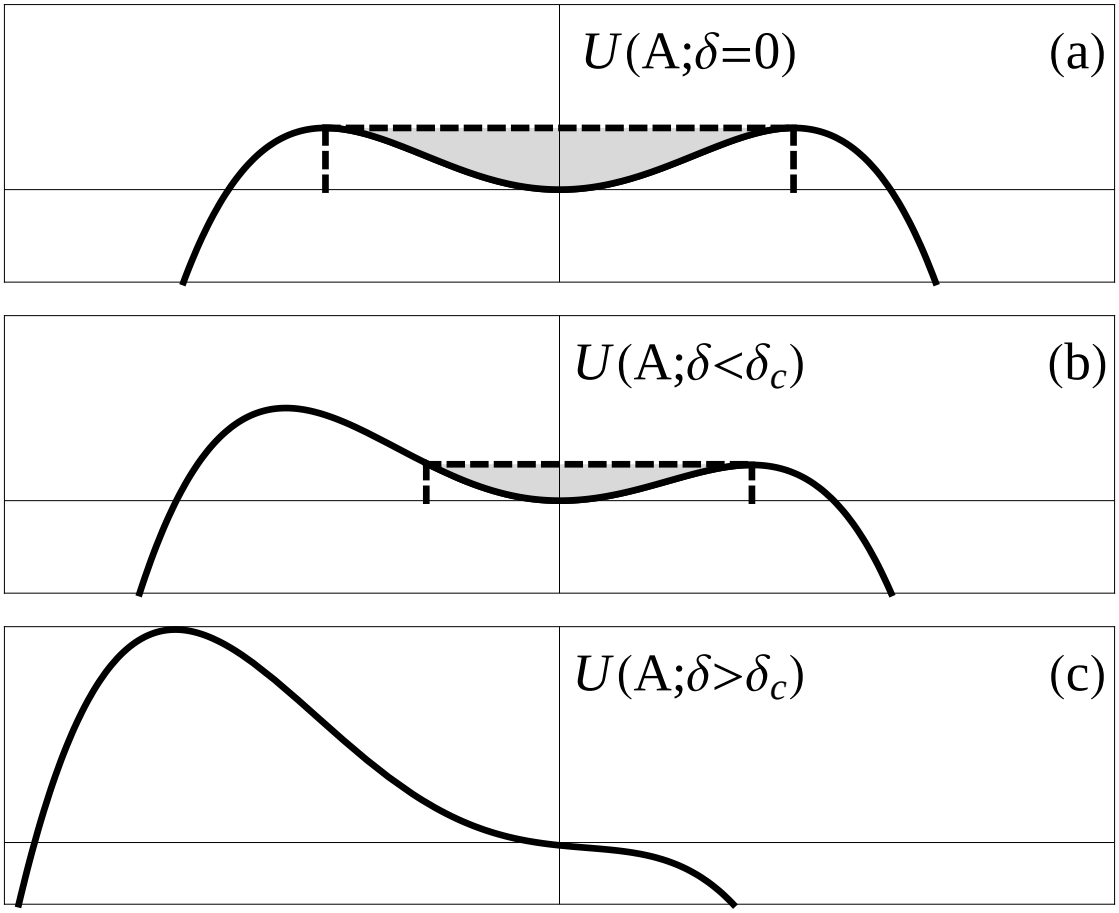

Figure 5.2: Plot of the potential energy $U(A;\delta)$ as a function of amplitude, A, for: (a) $\delta = 0$; (b) $\delta < \delta_c$; and (c) $\delta > \delta_c$. The dotted box shows the shrinking boundaries of the stable well (shaded region).

The above equation represents a potential energy as a function of A, given k, b and δ, and determines the overall stability of the system. We have chosen $b > 0$, to be marginally stable, and so, for $k^2 < 3$ the system is stable to all perturbations. However, for $k^2 > 3$ and fixed b the stability of the system is dependent on the size of δ and $A_0 = A(t = 0)$.

The potential, with $k^2 > 3$ and fixed b, is shown in Fig. 5.2 for different values

of δ. For $\delta = 0$ (Fig. 5.2a), there is a stable well for $|A_0| < A_c$, where

$$A_c = 2\sqrt{2}\sqrt{\frac{k^2+1}{k^2-3}} \times b^{1/2}. \tag{5.39}$$

This result is the same as the one found in Chapter 3 where nonlinear stability was noted and simulated for large enough A. As δ is increased the stable well shrinks as the two positive roots of $U'(A;\delta)$ merge. From Fig. 5.2b we can see that the symmetry of the potential is broken and one side of the stable well drops so that the critical A_0 to stay nonlinearly stable is less than the one given in Eq. (5.39). When $\delta = \delta_c$, where

$$\delta_c = \frac{\pi}{2}\sqrt{\frac{32}{27}\frac{(k^2+1)^3}{k^2-3}} \times b^{3/2}, \tag{5.40}$$

the positive roots of $U'(A;\delta)$ become degenerate and the stable well becomes a point. When $\delta > \delta_c$ (Fig. 5.2c) the system is always unstable for any A_0. This means that, even though the system is linearly stable, a boundary perturbation of order $(b/B_c)^{3/2}$ can precipitate a response in the plasma of much larger amplitude, of order $(b/B_c)^{1/2}$, accompanied by explosive growth.

We remark that, in this calculation, we have assumed the density gradient, ρ_0', to be constant. This is done for simplicity, to illustrate the two phenomena of amplification and nonlinear instability in a transparent manner. We showed in the previous chapter that ρ_0' constant is a reasonable simplification, and that keeping a general $\rho_0(x)$ (Chapter 3) did not result in new phenomena or mitigate the appearance of the foregoing phenomena.

5.4 Summary and Conclusions

We have shown that for systems operating close to marginal stability for the interchange mode, a small perturbation on the boundary can induce a large response in the core of the plasma. A simple linear analysis shows that a secondary equilibrium, with amplitude inversely proportional to the marginal stability parameter, can exist as boundary perturbations are added adiabatically. In addition, we showed that the boundary perturbations can penetrate deep inside the plasma to induce a global amplification. This suggests that the system would need to be far enough away from criticality so as to stay well-defined. We accordingly extend this analysis nonlinearly to show that, even if the perturbation were scaled much smaller than the marginal stability parameter, the system can become nonlinearly unstable for boundary perturbations larger than a critical value.

These results have implications in the stability analysis and corresponding design of magnetic confinement devices operating close to marginal conditions. With $\Delta\beta > 0$, a linear stability analysis would show that the system is stable to all perturbations; however, relatively much smaller boundary perturbations, of order $(\Delta\beta/\beta_c)^{3/2}$, can destabilize the system nonlinearly, with subsequent perturbations growing without small amplitude saturation. The results show that it is important to take into account these field perturbations in the stability analysis if one were to continue operating close to marginal conditions. Additionally, the strength and precision of the coils would have to be balanced in order to have stable system with large enough b to stabilize possible δ perturbations.

Chapter 6

Concluding Remarks

6.1 Summary of Results

We have shown that the interchange mode, near marginal stability, can exhibit different, nonlinear behaviour depending on the form of the perturbation. Much of what was known and established is in the confines of linear theory, away from marginal stability. It was well-known that there existed a sharp boundary to determine when perturbations would be stable or unstable – the β limit, β_c. We showed that the boundary is not as sharp as previously thought and that the question of stability is not as straightforward when $\Delta\beta = 1 - \beta/\beta_c$ is small. More importantly, the behaviour is different if the system is marginally stable, i.e. $\Delta\beta \gtrsim 0$, when linear theory predicts that the system is stable to all small perturbations. The analyses were done using reduced MHD equations in an idealized system with slab geometry and a gravitational term modelling the force due to magnetic curvature.

First we showed that with two-dimensional, marginally stable systems it was possible to become nonlinearly unstable when the initial perturbation was large enough. Stabilization of the interchange mode was achieved by introducing a transverse magnetic field that created field line bending to balance the linear Rayleigh-Taylor destabilization. The perturbation was introduced as an initial value that were allowed to evolve in time. It was found that perturbations of order $\Delta\beta^{1/2}$ were

large enough to nonlinearly destabilize the system. The result was supported by a nonlinear numerical MHD simulation where good agreement was found for $\Delta\beta$ of up to 10%.

We then showed that three-dimensional, marginally stable systems exhibited two different behaviours depending on the form of the perturbation used. Like the 2D case, perturbations were introduced as an initial value that was allowed to evolve in time, but unlike the 2D case, stabilization was accomplished by boundary conditions in the z direction that allowed for finite parallel wavenumber. Two different forms of the perburbations, called isomorphic and blob-like modes, were analyzed. It was found that the isomorphic modes exhibited the same nonlinear instability as the 2D case; however, the blob-like modes did not have the same nonlinear behaviour and remained stable. Because the blob-like modes could also satisfy line-tied boundary conditions, this meant that the line-tied interchange mode did not become nonlinearly unstable when marginality was approached.

Finally, we showed that the two-dimensional system exhibited a different behaviour when the boundary was perturbed instead of the plasma itself. It was found that as $\Delta\beta$ approached zero, small distortions on the boundary became amplified in the bulk of the plasma. We showed that this amplification was inversely proportional to $\Delta\beta$ and that it was a global phenomenon. Additionally, it was found that the combination of the amplification and nonlinearity resulted in a nonlinear instability. We showed that the induced instability was highly sensitive to boundary distortions and the system could go unstable to boundary perturbations of order $\Delta\beta^{3/2}$.

6.2 Significance of Results

This nonlinear instability result implies that there could be an issue with magnetic confinement systems designed to operate close to the β limit. Even if the system was designed to be linearly stable, relatively small perturbations can still cause a destabilization through this nonlinear effect. Even worse, the nonlinear result using boundary perturbations place an even stricter constraint on the maximum β. The amplitude of the boundary distortion required to induce the nonlinear instability is significantly smaller than the amplitude of perturbations required. These nonlinear effects would have to be considered in the design of magnetic confinement systems for fusion.

These results could also be used to explain the onset of disruptions in certain astrophysical systems. However, because these systems are usually stabilized by line-tying, it is less likely that this is the case. Even though this type of nonlinear instability could explain such an onset, it was found that it does not occur in the instance of line-tied boundary conditions.

6.3 Limitations of Analyses and Future Work

We reiterate that because the analyses were done using a model system, a number of key effects that are relevant to the stability of the interchange mode are excluded. For example, the effects of magnetic shear are not taken into account and it is likely that this could take a significant role in determining the overall stability of the system. Also missing from the analyses is the effect of curvature in the magnetic

geometry, the details of which are important in more complicated instabilities, e.g. ballooning modes. Finally, because the analyses were done with reduced equations, effects of compressibility and variations in the parallel magnetic field could not be included. Both of these effects might alter the nonlinear behaviour, but it is unclear as to exactly how it'll be affected. Overall this means that the analyses lacked the details of realistic geometry.

Despite these limitations, the analytical methods used produced some results that have not been seen in the interchange mode literature and, in some cases, were able to reproduce similar results from more complicated analyses. In this way, it is worthwhile to expand the analysis to account for some of these limitations or to investigate new problems. The results suggest consideration of extending the MHD Energy Principle to include boundary induced perturbations and ideal nonlinearities when close to marginal stability. Having a generalized energy principle that included these effects would prove useful in determining the stability of a specific magnetic confinement design. In general, the stability of an equilibrium for the purposes of designing a containment device is determined using an energy principle calculation. Outside of magnetic confinement, it would also be worthwhile to determine the applicability of the results to astrophysical systems.

Appendix A

Additional Calculations

This Appendix shows the details of how to derive Eqs. (3.33)-(3.35).

In simplifying Eq. (3.31), we found the functional, $\mathcal{F}[\psi_1, \psi_2]$, to be

$$\begin{aligned}\mathcal{F}[\psi_1, \psi_2] =& \frac{g}{B_c^2}\rho_0''\partial_y(\psi_1\psi_2) + \frac{1}{6}\frac{g}{B_c^3}\rho_0'''\partial_y(\psi_1^3) \\ &+ \mathbf{B}_1 \cdot \nabla_\perp \nabla_\perp^2 \psi_2 + \mathbf{B}_2 \cdot \nabla_\perp \nabla_\perp^2 \psi_1. \end{aligned} \tag{A.1}$$

The above equation can be simplified by writing ψ_1 and ψ_2 a certain way. From Eq. (3.24) we can write

$$\psi_2 = \tilde{\psi}_2 + \bar{\psi}_2 \tag{A.2}$$

where

$$\tilde{\psi}_2 = A(t)^2 \zeta_2(x) \cos(2ky). \tag{A.3}$$

Writing ψ_2 in this way, we get the following results

$$\partial_y \psi_2 = \partial_y \tilde{\psi}_2, \tag{A.4}$$

$$\nabla_\perp^2 \tilde{\psi}_2 = -\frac{g}{B_c^2}\rho_0' \tilde{\psi}_2 - \frac{g}{B_c^3}\rho_0'' \widetilde{\psi_1^2}, \tag{A.5}$$

where we have written $\psi_1^2 = \widetilde{\psi_1^2} + \overline{\psi_1^2}$ and

$$\widetilde{\psi_1^2} = \frac{1}{2} A(t)^2 \zeta_1(x)^2 \cos(2ky), \tag{A.6}$$

$$\overline{\psi_1^2} = \frac{1}{2} A(t)^2 \zeta_1(x)^2. \tag{A.7}$$

The result given by Eq. (A.5) can be derived by multiplying Eq. (3.25) with $A(t)^2\cos(2ky)$ and recombining the terms. Similarly, if we multiply Eq. (3.17) by $A(t)\cos(ky)$, we find that

$$\nabla_\perp^2\psi_1 = -\frac{g}{B_c^2}\rho_0'\psi_1. \tag{A.8}$$

Since $\mathbf{B}\cdot\nabla_\perp\psi = 0$ for all orders, we get that

$$\begin{aligned}\mathbf{B_1}\cdot\nabla_\perp\psi_1^2 &= 2\psi_1(\mathbf{B_1}\cdot\nabla_\perp\psi_1)\\ &= 0\\ &= \mathbf{B_1}\cdot\nabla_\perp(\widetilde{\psi_1^2}+\overline{\psi_1^2}),\end{aligned} \tag{A.9}$$

and therefore

$$\begin{aligned}\mathbf{B_1}\cdot\nabla_\perp\widetilde{\psi_1^2} &= -\mathbf{B_1}\cdot\nabla_\perp\overline{\psi_1^2}\\ &= \partial_y\psi_1\overline{\psi_1^2}\,',\end{aligned} \tag{A.10}$$

Similarly, since

$$\begin{aligned}\mathbf{B_1}\cdot\nabla_\perp\psi_2 + \mathbf{B_2}\cdot\nabla_\perp\psi_1 &= 0\\ &= \mathbf{B_1}\cdot\nabla_\perp(\tilde{\psi}_2+\bar{\psi}_2)\\ &\quad + \mathbf{B_2}\cdot\nabla_\perp\psi_1\end{aligned} \tag{A.11}$$

then it follows that

$$\begin{aligned}\mathbf{B_1}\cdot\nabla_\perp\tilde{\psi}_2 + \mathbf{B_2}\cdot\nabla_\perp\psi_1 &= -\mathbf{B_1}\cdot\nabla_\perp\bar{\psi}_2\\ &= \partial_y\psi_1\bar{\psi}_2'.\end{aligned} \tag{A.12}$$

We can now simplify the last two terms in Eq. (A.1). Using Eq. (A.2) we have

$$\begin{aligned}
\mathbf{B}_1 \cdot \nabla_\perp \nabla_\perp^2 \psi_2 &= \mathbf{B}_1 \cdot \nabla_\perp \nabla_\perp^2 (\tilde{\psi}_2 + \bar{\psi}_2) \\
&= \mathbf{B}_1 \cdot \nabla_\perp (-\frac{g}{B_c^2} \rho_0' \tilde{\psi}_2 - \frac{g}{B_c^3} \rho_0'' \widetilde{\psi_1^2}) \\
&\quad + \mathbf{B}_1 \cdot \nabla_\perp \bar{\psi}_2{}'' \\
&= -\frac{g}{B_c^2} \rho_0' \mathbf{B}_1 \cdot \nabla_\perp \tilde{\psi}_2 + \frac{g}{B_c^2} \rho_0'' \partial_y \psi_1 \tilde{\psi}_2 \\
&\quad - \frac{g}{B_c^3} \rho_0'' \mathbf{B}_1 \cdot \nabla_\perp \widetilde{\psi_1^2} + \frac{g}{B_c^3} \rho_0''' \partial_y \psi_1 \widetilde{\psi_1^2} \\
&\quad - \partial_y \psi_1 \bar{\psi}_2''',
\end{aligned} \tag{A.13}$$

where we used Eq. (A.5), and took advantage of the fact that $\bar{\psi}_2$ has no y dependence, to remove the Laplacians. Similarly, we use Eq. (A.8) to get

$$\begin{aligned}
\mathbf{B}_2 \cdot \nabla_\perp \nabla_\perp^2 \psi_1 &= \mathbf{B}_2 \cdot \nabla_\perp (-\frac{g}{B_c^2} \rho_0' \psi_1) \\
&= -\frac{g}{B_c^2} \rho_0' \mathbf{B}_2 \cdot \nabla_\perp \psi_1 + \frac{g}{B_c^2} \rho_0'' \partial_y \tilde{\psi}_2 \psi_1,
\end{aligned} \tag{A.14}$$

where we used Eq. (A.4) to get the second term.

Combining Eqs. (A.13) and (A.14) we can use Eqs. (A.10) and (A.12) to further simplify the terms with a gradient operator. So finally we get

$$\begin{aligned}
\mathbf{B}_1 \cdot \nabla_\perp \nabla_\perp^2 \psi_2 + \mathbf{B}_2 \cdot \nabla_\perp \nabla_\perp^2 \psi_1 &= -\frac{g}{B_c^2} \rho_0' \partial_y \psi_1 \bar{\psi}_2' \\
&\quad - \frac{g}{B_c^3} \rho_0'' \partial_y \psi_1 \overline{\psi_1^2}{}' + \frac{g}{B_c^2} \rho_0'' \partial_y (\psi_1 \tilde{\psi}_2) \\
&\quad + \frac{g}{B_c^3} \rho_0''' \partial_y \psi_1 \widetilde{\psi_1^2} - \partial_y \psi_1 \bar{\psi}_2'''.
\end{aligned} \tag{A.15}$$

We can also rewrite the first term of Eq. (A.1),

$$\frac{g}{B_c^2} \rho_0'' \partial_y (\psi_1 \psi_2) = \frac{g}{B_c^2} \rho_0'' \partial_y (\psi_1 \tilde{\psi}_2) + \frac{g}{B_c^2} \rho_0'' \bar{\psi}_2 \partial_y \psi_1. \tag{A.16}$$

We can now substitute for ψ_1, $\bar{\psi}_2$, $\tilde{\psi}_2$, $\widetilde{\psi_1^2}$ and $\overline{\psi_1^2}$ using Eqs. (3.16), (3.30), (A.3), (A.6), and (A.7). As described in Sec. 3.2.3, we use the operator $\int dx\, \zeta_1(x) \int d(cos(ky))$ on Eq. (3.31) in order to extract the terms that have a $\sin(ky)$ dependence. The other terms will be irrelevant since the integration will evaluate to zero if the dependence does not match. And so we find that

$$\begin{aligned}\int d(cos(ky))\mathcal{F}[\psi_1,\psi_2] = \pi k A(t)^3 \Bigg\{ & \frac{g}{B_c^2}\rho_0''\zeta_1\zeta_2 \\ & - \frac{1}{4}\frac{g}{B_c^3}\left(\rho_0'\zeta_1(\zeta_1^2)'' + \rho_0''\zeta_1(\zeta_1^2)' + \frac{1}{2}\rho_0'''\zeta_1^3\right) \\ & - \frac{1}{4}\frac{1}{B_c}\zeta_1(\zeta_1^2)''''\Bigg\} \end{aligned} \tag{A.17}$$

Finally, we use the operator $\int dx\, \zeta_1(x)$ on the above equation to get

$$\begin{aligned}\int dx\, \zeta_1(x) \int d(cos(ky))\mathcal{F}[\psi_1,\psi_2] = \pi k L_\rho A(t)^3 \times \\ \left(\frac{g}{B_c^2}\langle\rho_0''\zeta_1^2\zeta_2\rangle - \frac{1}{4}\frac{g}{B_c^3}\langle\rho_0'\zeta_1^2(\zeta_1^2)''\rangle \right. \\ \left. -\frac{1}{4}\frac{1}{B_c}\langle\zeta_1^2(\zeta_1^2)''''\rangle\right). \end{aligned} \tag{A.18}$$

We made use of the fact that $\zeta_1(x)$ decays exponentially at the boundaries to combine the three terms proportional to g/B_c^3 in Eq. (A.17) into one term through integration by parts.

To complete the derivation of Eqs. (3.33)-(3.35) we still need to simplify the rest of the terms. It is easy to see that after using the annihilation operator then we get

$$\begin{aligned}\int dx\, \zeta_1(x) \int d(cos(ky))(-2\frac{g}{B_c^2}b_2\rho_0'\partial_y\psi_1) = \\ - 2\pi k L_\rho A(t)\frac{g}{B_c^2}b_2\langle\rho_0'\zeta_1^2\rangle. \end{aligned} \tag{A.19}$$

Applying the same operator, we find that

$$\begin{aligned}
&\int dx\,\zeta_1(x)\int d(cos(ky))B_c\mathcal{L}(\psi_3)\\
&\qquad = -kB_c\int dy\int dx\,\zeta_1\sin(ky)\big(\nabla_\perp^2\psi_3+\frac{g}{B_c^2}\rho_0'\psi_3\big)\\
&\qquad = -kB_c\int dy\int dx\,\Big(\zeta_1''\sin(ky)\psi_3\\
&\qquad\qquad +\zeta_1(-k^2\sin(ky))\psi_3+\zeta_1\sin(ky)\frac{g}{B_c^2}\rho_0'\psi_3\Big)\\
&\qquad = -kB_c\int dy\int dx\,\sin(ky)\psi_3\times\\
&\qquad\qquad \big(\zeta''-k^2\zeta_1+\frac{g}{B_c^2}\rho_0'\zeta_1\big),
\end{aligned}\tag{A.20}$$

and therefore, using Eq. (3.17),

$$\int dx\,\zeta_1(x)\int d(cos(ky))B_c\mathcal{L}(\psi_3)=0.\tag{A.21}$$

We, once again, took advantage of the boundary conditions to perform some integration by parts to arrive at the above result. Lastly, the operator on the left-hand side of Eq. (3.31) gives

$$\begin{aligned}
&\int dx\,\zeta_1(x)\int d(cos(ky))(\frac{g}{B_c^2}\rho_0\rho_0'\partial_y\psi_1-\rho_0'\partial_y\psi_1')\\
&\qquad = \pi kL_\rho A(t)(\frac{g}{B_c^2}\langle\rho_0\rho_0'\zeta_1^2\rangle-\langle\rho_0'\zeta_1\zeta_1'\rangle)\\
&\qquad = \pi kL_\rho A(t)\frac{g}{B_c^2}\langle\rho_0\rho_0'\zeta_1^2\rangle,
\end{aligned}\tag{A.22}$$

where the second term was thrown away since it evaluates to zero due to the parity of the equilibrium density.

Collecting the terms given by Eqs. (A.18), (A.19), (A.21) and (A.22) together, we arrive at Eq. (3.32).

Appendix B

Description of Numerical Simulation

This Appendix presents the equations solved by the numerical simulation used in Chapter 3.

The two-dimensional numerical simulation solves the following equations:

$$\partial_t \rho + \nabla_\perp \cdot (\rho \mathbf{u}_\perp) - D_\rho \nabla_\perp^2 \rho = S, \tag{B.1}$$

$$\partial_t (\rho \mathbf{u}_\perp) + \nabla_\perp \cdot (\rho \mathbf{u}_\perp \mathbf{u}_\perp) - \mu \nabla_\perp^2 (\rho \mathbf{u}_\perp) = \mathbf{F}_\perp, \tag{B.2}$$

$$\partial_t (\rho u_z) + \nabla_\perp \cdot (\rho u_z \mathbf{u}_\perp) - \mu \nabla_\perp^2 (\rho u_z) = [B_z, \psi], \tag{B.3}$$

$$\partial_t B_z + \nabla_\perp \cdot (B_z \mathbf{u}_\perp) - \eta_\perp \nabla_\perp^2 B_z = [\psi, u_z], \tag{B.4}$$

$$\partial_t \psi + \mathbf{u}_\perp \cdot \nabla_\perp \psi - \eta \nabla_\perp^2 \psi = 0, \tag{B.5}$$

where $[f, h] \equiv \partial_x f \partial_y h - \partial_x h \partial_y f$ and

$$\mathbf{F}_\perp = -\nabla_\perp \left(\frac{T_0}{M} \rho + \frac{B_z^2}{2} \right) - \nabla_\perp \psi \nabla_\perp^2 \psi - \rho g \hat{\mathbf{x}}, \tag{B.6}$$

$$S = \eta_\perp S_0 \left(e^{-(x-x_1)^2/2\sigma^2} - e^{-(x-x_2)^2/2\sigma^2} \right). \tag{B.7}$$

The system is initialized with $\rho = 1$ and $B_z = 1$. We use $T_0/M = 0.3$ for the temperature and $g = 0.15$ for the gravitational acceleration. The Gaussian function sources have amplitude $S_0 = 4.5$, width $\sigma^2 = 6.25 \times 10^{-4}$ and are centered around $x_1 = 0.7$ and $x_2 = 0.38$ (where $L_x = 1$). The values are chosen by trial and error to

create a good $\rho_0'(x)$ profile for the simulation. The relative strength of the dissipation terms are as follows:

$$\mu = \eta = 5 \times 10^{-4},$$

$$\eta_\perp = 10^{-1}\eta,$$

$$D_\rho = 10^{-3}\mu.$$

The dissipation in the density, D_ρ, is for numerical stability and is made orders of magnitude smaller than the viscosity μ. As mentioned in Sec. 3.3 the B_z resistivity, $\eta_\perp$, is made smaller than η and μ in order to keep B_y approximately constant. The crossfield particle diffusion is set by $\eta_\perp$. Since the time and space scales are normalized to the Alfvén speed, V_{Az}, and the box size, L_x, the above coefficients imply a viscous magnetic Reynolds number of $\simeq 2 \times 10^3$ and a Lundquist number (for magnetic diffusion) of $\simeq 2 \times 10^4$.

For a detailed description of the algorithm see Ref. [41].

Appendix C

Isomorphic Calculation

This Appendix shows the explicit derivation of Eq. (4.37).

The equations for the isomorphic system are similar to the ones derived in Sec. 4.4 except using a different set of solutions for the lowest order equations. From Sec. 4.4, we found that the nonzero terms to lowest order satisfy the following equations

$$\partial_t \rho_1 = \rho_0' \partial_y \varphi_2, \tag{C.1}$$

$$\partial_t \psi_1 = B_c \partial_z \varphi_2, \tag{C.2}$$

$$B_c \partial_z \nabla_\perp^2 \psi_1 + g \partial_y \rho_1 = 0, \tag{C.3}$$

which, when combined, yield the eigenvalue equation

$$\mathcal{L}_{3D}(\varphi_2) \equiv (B_c^2 \partial_z^2 \nabla_\perp^2 + g\rho_0' \partial_y^2)\varphi_2 \tag{C.4}$$

$$= 0, \tag{C.5}$$

for φ_2. The modes we are interested in are the ones that have a structure given by Fig. 4.1b, i.e. we use the solution

$$\varphi_2 = \frac{1}{k_z B_c} \dot{A}(t) \sin(k_x x) \sin(k_y y + k_z z). \tag{C.6}$$

Substituting this solution into Eq. (C.5) gives the same condition for the critical magnetic field as given by Eq. (4.50), i.e.

$$B_c^2 k_z^2 (k_x^2 + k_y^2) = g\rho_0' k_y^2. \tag{C.7}$$

Solving for ρ_1 and ψ_1 by substituting Eq. (C.6) into Eqs. (C.1) and (C.2) yields

$$\rho_1 = \frac{\rho_0'}{B_c}\frac{k_y}{k_z}A(t)\sin(k_x x)\cos(k_y y + k_z z), \tag{C.8}$$

$$\psi_1 = A(t)\sin(k_x x)\cos(k_y y + k_z z). \tag{C.9}$$

Since this is a linear result and the solution for φ_2 given by Eq. (C.6) is just a linear combination of the solution used in Sec. 4.4 (Eq. (4.46)) it's not surprising that both calculations yield the same condition for B_c. The variation will enter when we introduce nonlinear terms.

From Sec. 4.4 we found that matching terms to next order yielded the following equations

$$\partial_t \rho_2 = \rho_0' \partial_y \varphi_3 + \{\rho_1, \varphi_2\}, \tag{C.10}$$

$$\partial_t \psi_2 = B_c \partial_z \varphi_3 + \{\psi_1, \varphi_2\}, \tag{C.11}$$

$$B_c \partial_z \nabla_\perp^2 \psi_2 + g\partial_y \rho_2 + \{\psi_1, \nabla_\perp^2 \psi_1\} = 0. \tag{C.12}$$

We now simplify the nonlinear terms by substituting Eqs. (C.6), (C.8), and (C.9) in the Poisson brackets. With this substitution, we find that

$$\{\rho_1, \varphi_2\} = \frac{1}{4}\frac{k_y^2}{k_z^2}\frac{k_x \rho_0'}{B_c^2}\partial_t(A(t)^2)\sin(2k_x x), \tag{C.13}$$

$$\{\psi_1, \varphi_2\} = \frac{1}{4}\frac{k_y}{k_z}\frac{k_x}{B_c}\partial_t(A(t)^2)\sin(2k_x x), \tag{C.14}$$

$$\{\psi_1, \nabla_\perp^2 \psi_1\} = 0. \tag{C.15}$$

Combining Eqs. (C.10)-(C.12) and the above equations yields the same equation for φ_3 as the one found in Sec. 4.4, i.e.

$$\mathcal{L}_{3D}(\varphi_3) = 0. \tag{C.16}$$

We can once again take

$$\varphi_3 = 0, \tag{C.17}$$

without loss of generality, and so we find that, like the 2D system, there is a second order average density and flux given by

$$\rho_2 = \bar{\rho}_2(t,x) = \frac{1}{4}\frac{k_y^2}{k_z^2}\frac{k_x\rho_0'}{B_c^2}A(t)^2\sin(2k_x x), \tag{C.18}$$

$$\psi_2 = \bar{\psi}_2(t,x) = \frac{1}{4}\frac{k_y}{k_z}\frac{k_x}{B_c}A(t)^2\sin(2k_x x). \tag{C.19}$$

These second order solutions match the 2D solutions found in Sec. 4.3, e.g. Eq. (4.32), using the condition for an isomorphism given by Eq. (4.36).

Continuing with the expansion, we get the same equations as Eqs. (4.66)-(4.68); however, there are extra terms because the isomorphic calculation has a nonzero second order flux. Keeping these terms, we get

$$\partial_t\rho_3 = \rho_0'\partial_y\varphi_4 + \{\rho_2,\varphi_2\}, \tag{C.20}$$

$$\partial_t\psi_3 = B_c\partial_z\varphi_4 + b_2\partial_z\varphi_2 + \{\psi_2,\varphi_2\}, \tag{C.21}$$

and

$$\begin{aligned}\partial_t(\rho_0'\partial_x\varphi_2 + \rho_0\nabla_\perp^2\varphi_2) = B_c\partial_z\nabla_\perp^2\psi_3 + g\partial_y\rho_3 + b_2\partial_z\nabla_\perp^2\psi_1 \\ + \{\psi_1,\nabla_\perp^2\psi_2\} + \{\psi_2,\nabla_\perp^2\psi_1\},\end{aligned} \tag{C.22}$$

as the full set of equations for the isomorphic case. To simplify the above equations, we start by applying ∂_t to Eq. (C.22) and substituting Eqs. (C.20) and (C.21) for

ψ_3 and ρ_3, respectively. After making some simplifications we get

$$\partial_t^2(\rho_0'\varphi_2' + \rho_0\nabla_\perp^2\varphi_2) = \mathcal{L}_{3D}(\varphi_4) + 2b_2B_c\partial_z^2\nabla_\perp^2\varphi_2 + (3k_x^2 - k_y^2)\partial_t\{\bar{\psi}_2, \psi_1\}$$
$$+B_c\nabla_\perp^2\{\bar{\psi}_2, \partial_z\varphi_2\} + g\{\bar{\rho}_2, \partial_y\varphi_2\}. \quad \text{(C.23)}$$

We annihilate φ_4 in the usual way of projecting Eq. (C.23) onto φ_2. The effect of this projection on the other terms is that only the components proportional to $\sin(k_x x)\sin(k_y y + k_z z)$ will remain after the operation. This is trivial since we have solutions for all the variables and so we can simplify easily to get

$$\frac{1}{k_z^2 V_{Ac}^2}\frac{d^2}{dt^2}A = -2\frac{b_2}{B_c}A + \frac{1}{4}\frac{k_y^2 - 3k_x^2}{k_x^2 + k_y^2}\frac{k_y^2}{k_z^2}\frac{A^3}{B_c^2/k_x^2} \quad \text{(C.24)}$$

as the final nonlinear time evolution equation. This equation matches Eq. (4.37) from Sec. 4.4.

Bibliography

[1] J. D. Lawson. Some criteria for a power producing thermonuclear reactor. *Proceedings of the Physical Society B*, 70:6, 1957.

[2] Jeffrey P. Freidberg. *Ideal Magnetohydrodynamics*. Modern Perspectives in Energy. Plenum Press, New York, 1987.

[3] Richard F. Post. Controlled fusion research – An application of the physics of high temperature plasmas. *Reviews of Modern Physics*, 28:338, 1956.

[4] John David Jackson. *Classical Electrodynamics*. John Wiley & Sons, Inc., 1999.

[5] M. D. Kruskal and R. M. Kulsrud. Equilibrium of a magnetically confined plasma in a toroid. *Physics of Fluids*, 1:265, 1958.

[6] M. D. Kruskal and C. R. Oberman. On the stability of plasma in static equilibrium. *Physics of Fluids*, 1:275, 1958.

[7] J. L. Johnson, C. R. Oberman, R. M. Kulsrud, and E. A. Frieman. Some stable hydromagnetic equilibria. *Physics of Fluids*, 1:281, 1958.

[8] A. B. Hassam. *Fluid Theory of Plasmas*. University of Maryland Report. Physics Publication No. 87-037, 1985.

[9] H. R. Strauss. Nonlinear, three-dimensional magnetohydrodynamics of noncircular tokamaks. *Physics of Fluids*, 19:134, 1976.

[10] H. R. Strauss. Dynamics of high β tokamaks. *Physics of Fluids*, 20:1354, 1977.

[11] Steven C. Cowley and Mehmet Artun. Explosive instabilities and detonation in magnetohydrodynamics. *Physics Reports*, 283:185–211, 1997.

[12] D. T. Adler and A. B. Hassam. Divergent subcritical convection in magnetized plasma from assymetric sourcing. *Physics of Plasmas*, 12:062506, 2005.

[13] Jupiter Bagaipo, P. N. Guzdar, and A. B. Hassam. Nonlinear stability of the ideal magnetohydrodynamic interchange mode at marginal conditions in a transverse magnetic field. *Physics of Plasmas*, 18:122103, 2011.

[14] Jupiter Bagaipo and A. B. Hassam. Boundary induced amplification and nonlinear instability of interchange modes. *Physics of Plasmas (Letters)*, 20:020704, 2013.

[15] M. N. Rosenbluth and C. L. Longmire. Stability of plasmas confined by magnetic fields. *Annals of Physics*, 1:120, 1957.

[16] Lyman Spitzer, Jr. The stellarator concept. *Physics of Fluids*, 1:253, 1958.

[17] Russell M. Kulsrud. The interchange instability in the stellarator. *Physics of Fluids*, 6:904, 1963.

[18] H. Alfvén. Existence of electromagnetic-hydrodynamic waves. *Nature*, 150:405–406, 1942.

[19] P. A. Sweet. The neutral point theory of solar flares. In B. Lehnert, editor, *Electromagnetic Phenomena in Cosmical Physics*, volume 6 of *IAU Symposium*, page 123, New York, 1958. Cambridge University Press.

[20] E. N. Parker. Sweet's mechanism for merging magnetic fields in conducting fluids. *Journal of Geophysical Research*, 62:509, 1957.

[21] Lord Rayleigh. Investigation of the character of the equilibrium of an incompressible heavy fluid of variable density. In *Proceedings of the London Mathematical Society*, volume 14, pages 170–177, 1883.

[22] Sir Geoffrey Taylor. The instability of liquid surfaces when accelerated in a direction perpendicular to their planes. In *Proceedings of the Royal Society of London. Series A, Mathematical and Physical Sciences*, volume 201, pages 192–196, 1950.

[23] S. Gupta, J. D. Callen, and C. C. Hegna. Violating suydam criterion produces feeble instabilities. *Physics of Plasmas*, 9:3395, 2002.

[24] P. H. Rutherford, H. P. Furth, and M. N. Rosenbluth. Non-linear kink and tearing-mode effects in tokamaks. In *Plasma Physics and Controlled Nuclear Fusion Research*, volume II, page 553, Vienna, 1971. International Atomic Energy Agency.

[25] F. L. Waelbroeck. Nonlinear growth of the quasi-interchange instability. *Physics of Fluids B*, 1:499, 1989.

[26] A. D. Beklemishev. Nonlinear saturation of ideal interchange modes in a sheared magnetic field. *Physics of Fluids*, 3:1425, 1991.

[27] P. Zhu, C. C. Hegna, and C. R. Sovinec. Nonlinear growth of a line-tied g mode near marginal stability. *Physics of Plasmas*, 13:102307, 2006.

[28] P. Zhu, C. C. Hegna, C. R. Sovinec, A. Bhattacharjee, and K. Germaschewski. Intermediate nonlinear regime of a line-tied g mode. *Physics of Plasmas*, 14:055903, 2007.

[29] D. Pfirsch and R. N. Sudan. Nonlinear ideal magnetohydrodynamics instabilities. *Physics of Fluids*, 5:2052, 1993.

[30] Bergen R. Suydam. Stability of a linear pinch. In *Second United Nations International Conference on the Peaceful Uses of Atomic Energy*, volume 81, page 157, United Nations, Geneva, 1958.

[31] James F. Drake and Thomas M. Antonsen, Jr. Nonlinear reduced fluid equations for toroidal plasmas. *Physics of Fluids*, 27:898, 1984.

[32] J. W. Connor, R. J. Hastie, and J. B. Taylor. Shear, periodicity, and plasma ballooning modes. *Physical Review Letters*, 40:396–399, 1978.

[33] O. A. Hurricane, B. H. Fong, S. C. Cowley, F. V. Coroniti, C. F. Kennel, and R. Pellat. Substorm detonation. *Journal of Geophysical Research*, 104:10211–10231, 1999.

[34] H. R. Wilson and S. C. Cowley. Theory for explosive ideal magnetohydrodynamic instabilities in plasmas. *Physical Review Letters*, 92:175006, 2004.

[35] P. Zhu, A. Bhattacharjee, and K. Germaschewski. Intermediate nonlinear evolution of the parker instability: Formation of convection-induced discontinuities and absence of finite-time singularities. *Physical Review Letters*, 96:065001, 2006.

[36] A. H. Boozer. Error field amplification and rotation damping in tokamak plasmas. *Physical Review Letters*, 86:5059–5061, 2001.

[37] A. H. Boozer. *Plasma Confinement*, volume 10, page 680. Academic, New York, 1987.

[38] A. Reiman and D. Monticello. Tokamak error fields and locked modes. *Physics of Fluids B*, 3:2230–2235, 1991.

[39] Jong kyu Park, Allen H. Boozer, Jonathan E. Menard, Andrea M. Garofalo, Michael J. Schaffer, Richard J. Hawryluk, Stanley M. Kaye, Stefan P. Gerhardt, Steve A. Sabbagh, and NSTX Team. Importance of plasma response to nonaxisymmetric perturbations in tokamaks. *Physics of Plasmas*, 16:056115, 2009.

[40] R. M. Kulsrud and T. S. Hahm. Forced magnetic reconnection. *Physica Scripta*, 1982:525–528, 1982.

[41] P. N. Guzdar, J. F. Drake, D. McCarthy, A. B. Hassam, and C. S. Liu. Three-dimensional fluid simulations of the nonlinear drift-resistive ballooning modes in tokamak edge plasmas. *Physics of Fluids B*, 5:3712, 1993.